Deanticoagulated Heparins Mediate Goblet Cell Differentiation to Restore Mucosal Barrier for Ulcerative Colitis Therapy

Wei Hu[1, #], Zhen Kang Liu[1, #], Long Huang[1,2, #], Wen Zeng[2], Xiao Yi Ren[1], Yang Ji[3], Zheng Yang Song[1], Qin Xuan Zhou[1],Haihong Chen[1], Bing Xu[1,4], Can Yang Zhang[1,2,5,6], Chong Zhang[2,6], Zhen Qing Zhang[7], Hong Chao Zhang[8], Yun Sheng Yang[9], Ye Chen[10], Xuan Jiang[11, *], Yi Wang[2, *], Xin-Hui Xing[1,2,4,5, 6, *]

[1]Institute of Biopharmaceutical and Health Engineering, Shenzhen International Graduate School, Tsinghua University, Shenzhen 518055, China

[2]Key Laboratory for Industrial Biocatalysis, Ministry of Education, Institute of Biochemical Engineering, Department of Chemical Engineering, Tsinghua University, Beijing 100084, China

[3]School of Medicine, Southern University of Science and Technology, Shenzhen, Guangdong Province 518112, China

[4]Institute of Biomedical Health Technology and Engineering, Shenzhen Bay Laboratory, Shenzhen 518118, China

[5]Key Laboratory of Active Proteins and Peptides Green Biomanufacturing of Guangdong Higher Education Institutes，Tsinghua Shenzhen International Graduate School, Shenzhen 518055, China

[6]Center for Synthetic and Systems Biology, Tsinghua University, Beijing 100084, China

[7]Jiangsu Key Laboratory of Translational Research and Therapy for Neuro-Psycho-Diseases

21 and College of Pharmaceutical Sciences, Soochow University, Suzhou, Jiangsu 215021, China

22 [8]Department of Cardiovascular Surgery, Air Force Medical Center, Beijing 100142, China

23 [9]Department of Gastroenterology and Hepatology, Chinese PLA General Hospital, Beijing

24 100853, China

25 [10]Department of Gastroenterology, Southern Medical University Shenzhen Hospital,

26 Shenzhen 518101, China

27 [11]Department of Gastroenterology, Beijing Tsinghua Changgung Hospital, Beijing 102218,

28 China

29

Abstract

Mucosal barrier dysfunction is a pathological hallmark of ulcerative colitis (UC), yet current clinical therapeutic strategies remain predominantly limited to anti-inflammatory therapies and/or surgical treatment, lack of reliable treatment for mucosal repairment[1,2]. Here, through a systematic screen of our established library for deanticoagulated heparins[3], we found that the nonanticoagulant low-molecular-weight heparin NALHP with average Mw 6400 Da and its separated representative fine fragment S6 with average Mw 4200 Da with similar structures exhibited marked therapeutic efficacy for dextran sulfate sodium (DSS)-induced UC mice by ameliorating the pathological phenotypes and repairing intestinal damage. NALHP and S6 were found to specifically mediate differentiation of the crypt stem cells into goblet cells in UC mice, and promote restoration of the damaged mucosal barrier. Notably, using human UC patient-derived organoid models, NALHP and S6 were mechanistically demonstrated to reconstruct the cellular composition profiles, and direct differentiation of the colonic stem cells into goblet cells by regulating Wnt and Notch signaling pathways, thereby facilitating the mucus layer repair. Our study is the first to reveal the main mechanism of deanticoagulated heparins for UC therapy through specifically mediating goblet cell differentiation, providing crucial insights for development of novel UC therapeutics by targeting mucosal barrier repair process.

49 **Introduction**

50 Ulcerative colitis (UC) is a chronic, idiopathic, and intractable disease that recurrently and
51 continuously triggers inflammation of the colonic mucosa[4-6] and is among the principal
52 inflammatory bowel diseases. Clinically, UC patients frequently exhibit symptoms such as
53 abdominal pain, loose stools, abscesses and bloody stools, low-grade fever, and malnutrition[5,7],
54 which can render them completely incapable of working and, further, potentially induce colon
55 cancer[8,9]. Although more than 160 years have passed since the first case of UC was reported in
56 the literature, there is still no clear and unified pathogenetic mechanism of UC. This lack is
57 attributed mainly to the complex pathogenesis and influencing factors of UC. It is generally
58 acknowledged that immunity, genes, the environment, and the gut microbiota are the four major
59 factors influencing the incidence of UC and that these four factors interact and jointly facilitate
60 the progression of UC. The complex and unknown pathogenesis of UC also poses difficulties and
61 challenges for drug development and clinical treatment. However, the main pathological feature
62 of UC at the endoscopic and molecular levels is substantial intestinal barrier damage, including
63 damage to the intestinal epithelial barrier and the mucous layer barrier, at the site of ulceration[2].
64 Mucosal healing is an important clinical hallmark indicating the efficacy of UC treatment[1].
65 However, currently, the clinical treatment of UC mainly encompasses anti-inflammatory drug
66 therapy and/or surgical treatment[10]. Moreover, none of the existing treatments can completely
67 cure UC. More specifically, no treatment method can achieve complete tissue healing in the
68 mucosal layers of UC patients[2]. Given that there is currently no specific drug for UC treatment,

69 drug therapy regimens for UC generally consist of broad-spectrum anti-inflammatory drugs such
70 as nonsteroidal anti-inflammatory drugs, corticosteroids, immunosuppressants, and biologics[11].
71 Among these drugs, 5-aminosalicylic acid (5-ASA) drugs (mesalamine and olsalazine) are the
72 most widely utilized first-line clinical drugs for the anti-inflammatory treatment of UC[12]; these
73 drugs can begin to have effects within 2 to 4 weeks and alleviate the condition in approximately
74 53% of patients[13]. UC patients treated with corticosteroids (prednisone and budesonide), the
75 second-line drugs for UC treatment, have a remission rate of approximately 50%[14]. Biologics
76 (infliximab and adalimumab) are utilized for the treatment of patients with moderate to severe
77 UC and can directly act on inflammatory signaling pathways such as the tumor necrosis factor
78 alpha (TNF-α) and Janus kinase (JAK) pathways[15]. However, biologics are relatively costly, and
79 fewer than 30% of UC patients respond to biologic therapy[16]. Additionally, most of the new UC
80 drugs under development are biologics that act mainly on JAK, Sphingosine-1-Phosphate
81 Receptor 1 (S1P1), α4β7 integrin and other mediators to regulate immunity and inflammation[17].
82 However, these new drugs are unable to overcome the limitation of the 20% to 30% remission
83 rate of UC patients treated with biologics[2].
84 Heparin (HP) is a high-molecular-weight linear polysaccharide[18] with a complex molecular
85 structure characterized by an intricate sugar chain framework comprising alternating
86 glucosamine (GlcN) and hexuronic acid (HexA)—namely, glucuronic acid (GlcA) or iduronic
87 acid (IdoA)—units linked through α(1→4) or β(1→4) glycosidic bonds with elaborate acetyl and
88 sulfonic acid group modifications[19]. Owing to its highly sulfonated nature along with its intricate

89 sugar chain architecture[20], HP exhibits binding affinity for numerous proteins, leading to diverse
90 biological activities encompassing anticoagulant and other activities that have led to its clinical
91 application for more than 80 years[21], such as anti-inflammatory[22], antitumor[23], and antiviral[24]
92 activities. While the anticoagulant function of HP arises from specific pentasaccharide sequences
93 (GlcNS6S/GlcNAc6S-GlcA-GlcNS6S3S-IdoA2S-GlcNS6S) within its sugar chains that interact
94 with antithrombin III (ATIII), these sequences account for only approximately 30% of its
95 content, leaving much unexplored territory awaiting further investigation[20], and elucidating the
96 nonanticoagulant functions of HP remains pivotal in scientific value and the development of
97 next-generation HP drugs. A profound challenge in glycoscience is posed by the structural
98 complexity resulting from the presence of diverse monosaccharides and their modifications,
99 which form repetitive disaccharide units and complicate both structural and functional analyses.
100 Gaffney *et al.*[25] fortuitously discovered in 1995 that the combination of subcutaneous
101 anticoagulant HP drug injection and oral sulfasalazine administration in 10 patients with UC
102 refractory to traditional drug therapy alleviated the disease in 9 of the patients, thereby initiating
103 anticoagulant therapy with HP for UC[26]. However, studies on anticoagulant HP drug therapy for
104 UC often have limitations, such as inconsistent conclusions[27-29], a lack of clarity regarding the
105 effective molecular structure, unknown mechanisms of action and a high risk of massive
106 bleeding in UC lesions because of the anticoagulant activity[30], indicating that clinical HP drugs
107 with anticoagulant activity cannot be effective for UC therapy. However, one of the well-known
108 nonanticoagulant activities of HP, i.e., its specific targeting of integrin αM–mediated immune

109 cells at inflammatory sites, has been successfully used to develop oral bifunctional
110 nanotherapeutics that treat UC by ameliorating oxidative stress and inhibiting the activation of
111 inflammation-associated signaling pathways[29]. To address the problems of the instability of
112 anticoagulant HP drugs and the bleeding risk associated with their use in the treatment of UC, in
113 this paper, the deanticoagulated HP derivates library constructed by our group[3] was used for in
114 vitro and in vivo screening of anti-UC activity, and NALHP, a nonanticoagulant low-molecular-
115 weight HP with significant and stable treatment efficacy for UC, as determined by oral
116 administration to mice with DSS-induced UC, was discovered. Through discriminative analysis,
117 we discovered that NALHP, with an average molecular weight (Mw) of 6400 Da and a
118 polydispersity index (PDI) of 2.23, and its representative fine fragment S6 separated by gel
119 chromatography, with an average Mw of 4200 Da and a polydispersity index (PDI) of 1.1 and
120 accounting for 15.3% (w/w) of the content of NALHP, which was the highest among the
121 fragments, can be effectively used to treat UC in mice. Notably, NALHP and S6 significantly
122 restored the colonic mucosal barrier in UC mice by restoring the proliferation and differentiation
123 ability of colonic crypt stem cells. Furthermore, using human UC patient-derived colon
124 organoids, we elucidated the detailed mechanism through which NALHP and S6 increase the
125 proportion of functional cells, especially goblet cells, in the organoids by simultaneously
126 inhibiting the activity of the Wnt and Notch signaling pathways to promote the differentiation of
127 intestinal stem cells into goblet cells, thereby profoundly restoring the mucosal barrier.
128

Results

Deanticoagulated HPs: structural characterization

In clinical practice, the manufacturing process of anticoagulant HP drugs primarily aims to preserve the structural integrity of the anticoagulant pentasaccharide sequence. However, the enrichment of sequences with anticoagulant activity during production may disrupt or impair the more abundant nonanticoagulant sequences of HP molecules, thereby reducing the stability and reproducibility of their nonanticoagulant therapeutic efficacy in ulcerative colitis (UC). To more effectively investigate the consistent nonanticoagulant biological activity of HP, we previously established a library of different structurally modified deanticoagulated HP derivates, including NAHP, I-45, NAI45, and III,II-2-Odes-1[3], together with Eno (enoxaparin) and NAEno (deanticoagulated enoxaparin) (Fig. 1a). Using the well-established mouse model of 3% dextran sulfate sodium (DSS)-induced UC (Extended Data Fig. 1a), we evaluated the therapeutic efficacy of various deanticoagulated HP derivates in this library. As shown in Extended Data Fig. 1, nonanticoagulant HP (NAHP; average Mw, 13444 Da; PDI=1.28), an deanticoauglated HP derivates obtained through periodate oxidation followed by sodium borohydride reduction of heparin (HP; average Mw, 17928 Da; PDI=1.28), in which the glucuronic acid of the pentasaccharide unit was ring-opened, resulting in the loss of anticoagulant activity (Fig. 1a), exhibited stable efficacy in partially restoring the structure of the colon tissue (Extended Data Fig. 1b-g). However, the anticoagulant HP and the other four deanticoagulated HP derivates (I-

45, III,II-2-Odes-1, Eno and NAEno) prepared differently did not have this stable biological effect.

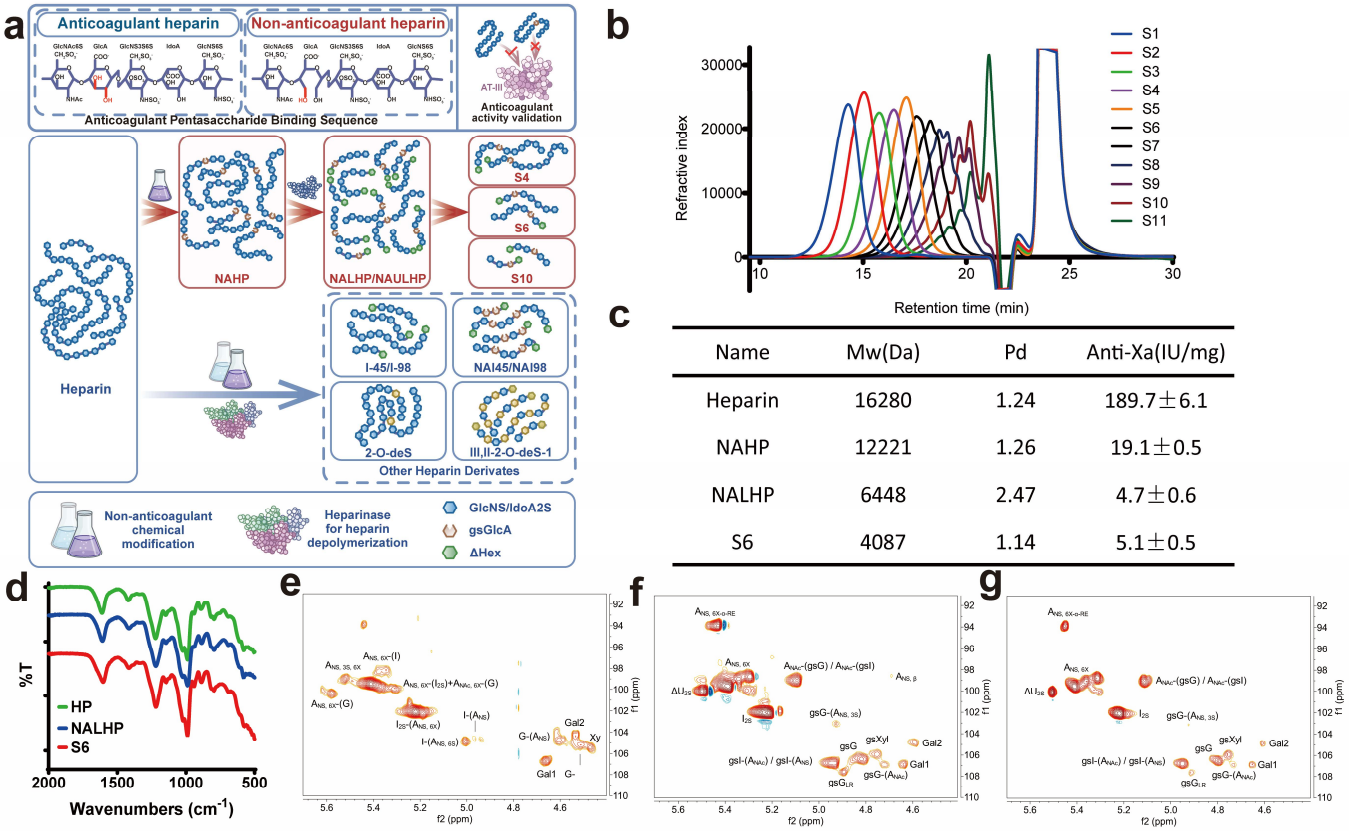

Name	Mw(Da)	Pd	Anti-Xa(IU/mg)
Heparin	16280	1.24	189.7±6.1
NAHP	12221	1.26	19.1±0.5
NALHP	6448	2.47	4.7±0.6
S6	4087	1.14	5.1±0.5

Fig. 1 Characterization of deanticoagulated HP derivates. a, A library of deanticoagulated HP derivates was constructed: NAHP (nonanticoagulant HP, prepared by periodate oxidation followed by sodium borohydride reduction of heparin), I-45 (prepared by enzymatic hydrolysis with heparinase I until the absorbance increased to 45), NAI45 (prepared by periodate oxidation followed by sodium borohydride reduction of I-45), III,II-2-Odes-1 (prepared by combined enzymatic hydrolysis with heparinase III and heparinase II)[3], Eno (enoxaparin) and NAEno (prepared by prepared by of enoxaparin). **b,** Molecular weight HPLC chromatograms of S1-S11. **c,** Physicochemical properties of HP and deanticoagulanted HP derivates. **d,** Infrared spectra of

160 HP and HP derivates. **e–g,** HSQC spectra of HP **(e)** and its derivates NALHP **(f)** and S6 **(g)**, A
161 represents GlcN, G represents GlcA, I represents IdoA, ΔU represents ΔHexA; in the sulfonic
162 acid group modification, X indicates that the sulfonic acid group modification at this position is
163 optional; the parentheses indicate the polysaccharide structure connected to the target sugar unit,
164 not the chemically attributed target sugar unit; RE represents the reducing end; LR represents the
165 GlcA-Gal-Gal-Xyl tetra saccharide structure existing in heparin, which is the linkage region for
166 diverse connection of serine residues of proteins in heparin.
167 Furthermore, compared with the first-line clinical drug 5-ASA, the respective nonanticoagulant
168 low-molecular-weight and ultra-low-molecular-weight HP derivates of NAHP, i.e., NALHP
169 (average Mw, 6400 Da; PDI=2.33) and NAULHP (average Mw, 3800 Da; PDI=4.15), which
170 were obtained via controlled enzymatic hydrolysis of NAHP with heparinase I (Fig. 1a),
171 demonstrated even more pronounced therapeutic efficacy in UC mice (Extended Data Fig. 2a-h).
172 Both NALHP and NAULHP significantly ameliorated DSS-induced damage to the colonic
173 mucosal barrier and facilitated the restoration of intestinal crypt architecture (Extended Data Fig.
174 2a-h). They also effectively reduced the serum concentrations of inflammatory cytokines (IL-6
175 and TNF-α) by more than 50% (Extended Data Fig. 2g and h). Notably, compared with
176 NAULHP, NALHP, which can be prepared in a stable form by the established production process
177 (Extended Data Fig. 3a-c and Extended Data Tables 3-5), showed greater efficacy in decreasing
178 DSS-induced mortality (Extended Data Fig. 2i). Therefore, NALHP was selected for all
179 subsequent investigations. In addition, we found that the adsorption and desorption curves of

180 DSS and HP, NAHP, NALHP, and NAULHP were consistent with those of the water control
181 group by the biofilm layer interference technique, confirming that there was no interaction
182 between HP derivates and DSS (Extended Data Fig. 2j and k).
183 Given the large difference in molecular weight between the enzymatic hydrolysis product
184 NALHP from NAHP (PDI=2.23 for NALHP vs. PDI=1.28 for NAHP), we performed fine
185 separation of NALHP using gel exclusion chromatography, collecting key fragments with an
186 average molecular weight difference of approximately 500 Da. A total of 11 distinct fractions
187 were obtained and designated S1 to S11 (Fig. 1a, b and Extended Data Table 1). Among these 11
188 separated fractions, S6, the intermediate-molecular-weight fraction of NALHP (Extended Data
189 Table 1, Extended Data Fig. 4c and d), with an average molecular weight of 4200 ± 150 Da
190 (PDI=1.1), exhibited bioactivity like that of NALHP (Fig. 1c and Extended Data Fig. 4). In
191 addition, S10 (average Mw, 1282Da; PDI=1.15) has no efficacy on mucosal remodeling. The
192 efficacy of NAULHP and S4 (average Mw, 6254Da; PDI=1.05) is inferior to that of NALHP and
193 S6. Structural characterization confirmed that S4 and S6 fully retained the characteristic
194 functional groups and sugar chain structure of the parent NALHP and NAULHP (Fig. 1d-g,
195 Extended Data Fig.5), but the main molecular structure of S10 is ΔHexA2S and the reducing end
196 is α-GlcNS6X, the Gal1, Gal2, Xyl and $GlcA_{LR}$ signal peaks in the LR region are missing
197 (Extended Data Fig.5). The above results together with the PCA of the UC treatment phenotypes
198 for HP, NAHP, NALHP, NAULHP, S4, S6 and S10 (Extended Data Fig.4j) indicate that in the
199 NALHP, the fragments with molecular weights ranging from 3000Da to 8000Da are the main

active components, and S6 is the representative fraction of NALHP with the similar biological activity and structure, which can also be stably prepared (Extended Data Fig.3d).

This consistent therapeutic efficacy of NALHP and S6 is markedly distinct from that of native HP. Consequently, we conducted a comparative structural analysis of UC-effective NALHP/S6 and UC-ineffective native HP, NAI45 and other HP derivates using Fourier transform infrared spectroscopy (FTIR) and two-dimensional nuclear magnetic resonance spectroscopy (2D-NMR). The results indicated that (1) the chemical modifications for deanticoagulation did not significantly alter the characteristic functional groups of the HP polysaccharide chain, such as the N-sulfate and O-sulfate groups (Fig. 1d, Extended Data Fig. 6-8, Extended Data Table. 2); (2) The main structural differences between HP and NAHP are the generation of an open-ring structure (Fig. 1e, Extended Data Fig. 5a) and the disappearance of the corresponding open-ring sites. The main structural differences between NAHP and NALHP and NAULHP are the production of the enzymatic product ΔHexA2S and the ability to distinguish the conformation of some polysaccharides. (Fig. 1f, Extended Data Fig. 5a, b); (3) The HSQC spectra of NALHP, NAULHP, S4 and S6 are similar in the shape, and the peak assignments are completely consistent, indicating the structural similarity among these four. This is also consistent with the biological activity phenotype for treating UC (Fig. 1f, g, Extended Data Fig. 5b, c) ;(4) As a small molecule oligosaccharide, the HSQC spectrum of S10 shows significant differences from S4 and S6. The spectral region of LR is missing the Gal1, Gal2, Xyl and $GlcA_{LR}$ signal peaks. Based on the peak height, it can be determined that the main molecular structure in S10 is

220 ΔHexA2S and the reducing end α-GlcNS6X. This indicates that S10 concentrates many
221 oligosaccharide fragments generated after the HepI degradation in NALHP. This is also
222 consistent with the fact that S10 only has limited biological activity for treating UC (Extended
223 Data Fig. 5d) ;(5) Compared with NAEno prepared from enoxaparin through deanticoagulation,
224 it has significant differences in the HSQC spectra compared with NAHP and NALHP with the
225 biological activity for treating UC. The LR region of Gal1, Gal2, Xyl and $GlcA_{LR}$ signal peaks
226 are not present in NAEno, and the α-GlcNS6X signal peak at the reducing end is also absent.
227 This is consistent with the performance of NAEno not having the biological activity for treating
228 UC (Extended Data Fig. 5e); (6) Compared with NALHP, NAI45 only has differences in the
229 preparation process sequence, i.e. first the enzymolysis then deanticoagulation, but this also
230 causes significant differences in the HSQC spectra between the two. NAI45 does not detect the
231 signal peaks of reducing end α-GlcNS6X, β-GlcNS, gsGlcA-(GlcNS3S) and gsGlcA-(GlcNAc)
232 in the spectrum, indicating the structural differences between NAI45 and NALHP. This may be
233 an important reason why NAI45 does not have the biological activity for treating UC (Extended
234 Data Fig. 5f).
235
236 ***Deanticoagulated HPs relieve UC pathology via mucosal repair***
237 The results obtained in the DSS-induced UC mice demonstrated that both NALHP and S6
238 significantly improved the pathological phenotypes (Fig. 2a). Specifically, they effectively
239 inhibited the weight loss of UC mice (Fig. 2b), restored the colon length to 92% of that in the

240 normal group (Fig. 2c and e), and reduced the abnormal increase in the spleen index by 40%
241 (Fig. 2d and f). Furthermore, both NALHP and S6 significantly suppressed the increase in the
242 serum concentrations of IL-6 and TNF-α, decreasing the final concentrations by 62% and 90%,
243 respectively (Fig. 2g and h). Histopathological analysis revealed that the colonic crypt structure
244 in the NALHP and S6 treatment groups was completely reconstructed (Fig. 2i4, i5 and j) and that
245 the goblet cell density was restored to more than 85% of that observed in the normal group (Fig.
246 2k4, k5 and l). These effects were significantly greater than those observed in the HP treatment
247 group (Fig. 2i3, k3 and j) and the positive control drug (5-ASA) group ($p < 0.01$) (Fig. 2i6 and
248 k6). The combined results of glycoprotein staining with WGA, EdU incorporation, and MUC2
249 immunohistochemical staining revealed marked restoration of the colonic mucus layer in the
250 NALHP and S6 groups (Fig. 2 m4 and m5), whereas no such restoration was observed in the HP
251 groups (Fig. 2m2 and m3). Slight restoration of the mucus layer was observed in the 5-ASA
252 group (Fig. 2m6), but the degree of restoration was much lower than that observed in the
253 NALHP and S6 groups. Additionally, the expression level of the mucin MUC2 in the NALHP
254 and S6 groups was significantly greater than that in the model group ($p < 0.001$) (Fig. 2l). EdU
255 incorporation assay results further confirmed that the intestinal epithelial cell proliferation index
256 was significantly greater in the treatment groups than in the model group ($p < 0.001$) (Fig. 2n),
257 whereas traditional drugs such as anticoagulant HP and the anti-inflammatory drug 5-ASA had
258 no significant reparative effects. Collectively, these findings indicate that treatment with either
259 NALHP or S6 can effectively repair mucosal injury in DSS-induced UC mice, restore the colonic

mucosal protein expression, and reconstruct the mucosal barrier. We also further explored the effects of the S6 administration method. Intravenous injection, intraperitoneal injection, and subcutaneous injection failed to achieve the effects of oral S6 in repairing the intestinal mucosal barrier of mice with DSS-induced colon damage (Extended Data Fig. 9). Oral administration is the best route for NALHP/S6 to exert their effects.

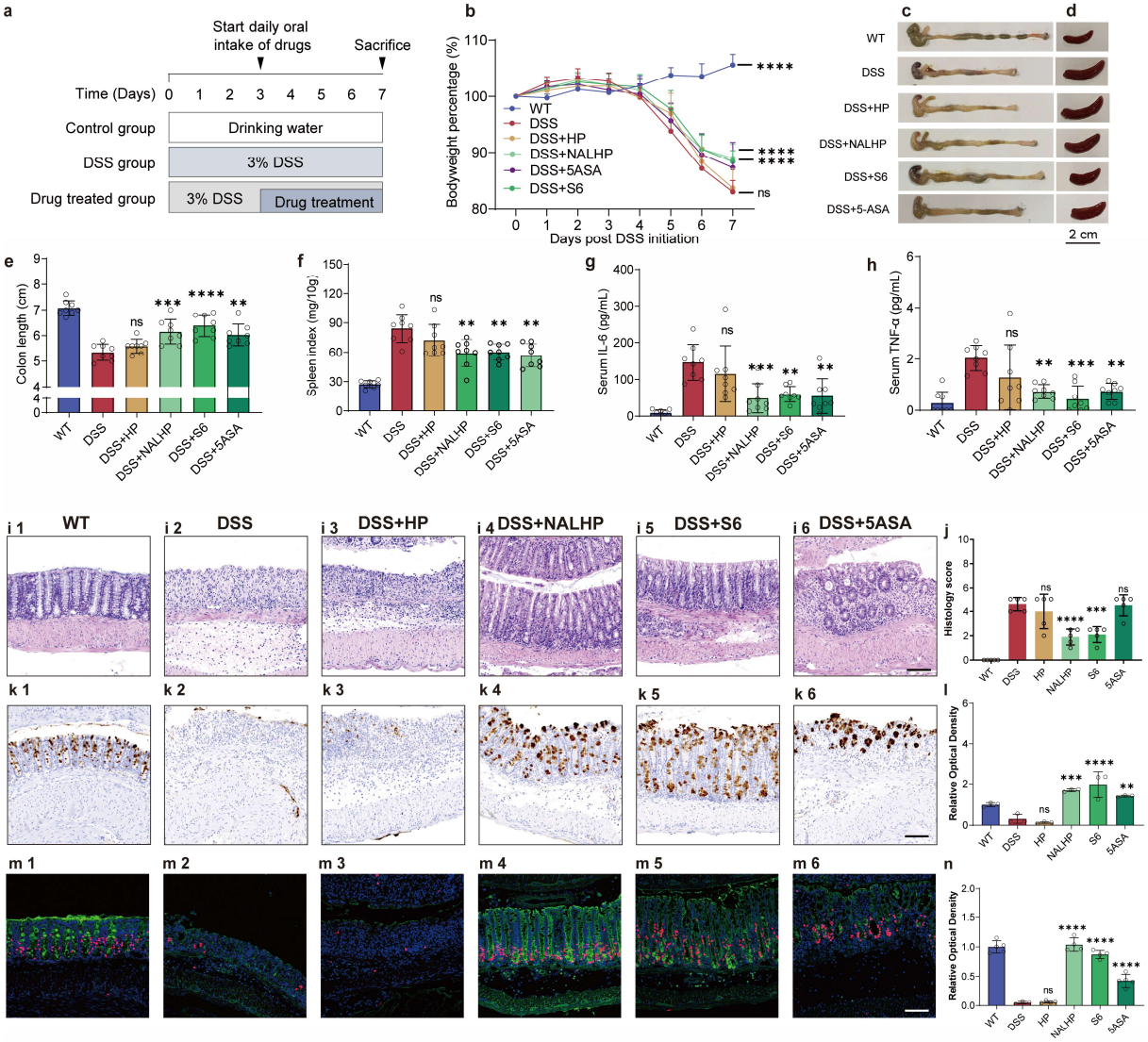

Fig. 2 Evaluation of the therapeutic efficacy of nonanticoagulated HP derivates. a, 3% DSS

267 was added to the drinking water for 7 days to induce acute colitis in mice (n=8). The mice in the
268 control group were given regular drinking water (n=8), and the mice in the drug treatment group
269 were given 30 mg/kg HP, NALHP, S6, or 5-ASA on the third day (n=8). **b,** Changes in weight.
270 **c–f,** Mice were sacrificed on day 7, and the colon (**c**) and spleen (**d**) were harvested. The colon
271 length (**e**) and the spleen index (**f**) were quantified. **g, h,** The serum concentrations of IL-6 (**g**)
272 and TNF-α (**h**) were determined by ELISA when the mice were sacrificed on day 7. **i1-i6.**
273 Representative images of colons stained with hematoxylin and eosin and their quantitative
274 histological scores (**j**). Scale bar, 100 μm. **k1-k6,** Representative images of colons stained with
275 hematoxylin and MUC2 and their quantitative immunohistochemical scores (**l**). Scale bar, 100
276 μm. **m1-m6,** Representative images of colons stained with EdU (red) and WGA (green) and their
277 quantitative immunohistochemical scores (**n**). Scale bar, 100 μm. Representative images or
278 quantitative analyses of n= 8 animals (**b-h**) and n=5 biologically independent samples (**i-n**) are
279 shown. The data are presented as the mean ± SD values. * $p < 0.05$, ** $p < 0.01$, *** $p < 0.001$,
280 **** $p < 0.0001$ and ns (not significant) $p > 0.05$; the data were analyzed by ordinary one-way
281 ANOVA (**b**) with multiple comparison testing.
282 To further elucidate the mechanism underlying NALHP- and S6-mediated mucosal barrier
283 restoration as described above, we employed multiomics approaches to analyzing the whole-
284 transcriptome and 16S rRNA profiles of the colon and colon contents in UC mice (Extended
285 Data Fig.10,11). The intestinal microbiota of UC mice mainly consists of potential pathogenic
286 bacteria such as *Bacteroides*, *Sutterella*, and *Turicibacter*, as well as the bacteria closely

287 associated with UC patient[31,32]. While, treatment with the deanticoagulated HP derivates,
288 especially NALHP, NAULHP, S6, NAEno and NAI45, all led to the characteristic intestinal
289 microbiota of the UC mice becoming similar as those of the WT mice (Extended Data Fig. 10a-
290 c). However, treatment with 5-ASA changed the intestinal microbiota composition of UC mice,
291 mainly consisting of *Pseudomonas*, *Neisseria*, *Thermicanus*, differently from those treated by the
292 deanticoagulated HP derivates and WT mice (Extended Data Fig. 10a-c). On the other hand,
293 metabolome analysis shows that both the deanticoagulated HP derivates and 5-ASA can alter the
294 metabolic profile of the colon contents in UC mice at the same time. Treatment with NAHP,
295 NALHP, NAULHP, S4, and S6 alleviated the accumulation of inflammatory-related metabolic
296 products and restored the composition of basic metabolic products, but treatment with HP, S10,
297 NAEno, NAI45 and 5-ASA failed to recover (Extended Data Fig. 10d-f). Both treatment with the
298 deanticoagulated HP derivates and 5-ASA can significantly change the transcriptome of colonic
299 epithelial cells in UC mice, altering the transcription of thousands of genes (Extended Data Fig.
300 11a). But through the analysis of phenotypic related differentially expressed genes, it was found
301 that the treatment of UC mice by the NALHP, NAULHP, S4, and S6 regulated the differentially
302 expressed genes related to metabolites, apoptosis, MAPK signaling pathway, and deeply
303 participated in the gene regulation of the inflammatory response and cell stemness, which was
304 different from the treatment effects of HP, S10, NAEno, NAI45 and 5-ASA on the transcriptome
305 of UC mice (Extended Data Fig. 11b). Further Gene Ontology (GO) analysis indicated that
306 mucosal barrier repair was a manifestation of the wound healing process, which was mediated

307 primarily through pathways such as the Wnt signaling pathway, which regulate intestinal
308 epithelial cell development and proliferation in UC mice after the treatment by the NALHP,
309 NAULHP, S4, and S6 (Extended Data Fig. 11c).
310 Based on the results of the multiomics analysis, the biological activities of the NAEno and
311 NAI45 in treating UC are inconsistent with their effects on the alteration of colonic metabolites
312 and intestinal flora. This indicates that the metabolites and intestinal flora are influenced by
313 multiple factors and are not the core targets of the effective treatment of UC mice. However, the
314 results of transcriptomics analysis suggest that NALHP and S6 may achieve disease relief in UC
315 mice by regulating cell stemness, inflammatory responses, cell connections, and the Wnt
316 signaling pathway (Extended Data Fig. 11b, c). During the active phase of UC, changes in
317 epithelial cell proliferation occur at the sites of colonic ulceration. Therefore, we selected PCNA
318 as a marker of cell proliferation and TCF1 as a downstream effector of the Wnt signaling
319 pathway. Immunohistochemical staining revealed that NALHP and S6 treatment normalized
320 PCNA expression following ulceration and restored TCF1 expression downstream of the Wnt
321 pathway, but these effects were not observed in UC mice treated with the anticoagulant HP or 5-
322 ASA (Extended Data Figs. 12 and 13). In conclusion, our results above suggest that NALHP and
323 S6 may restore the mucous barrier by restoring the proliferation and differentiation of colonic
324 crypt stem cells.
325
326 ***NALHP & S6 promote goblet cell differentiation in UC organoids***

327 Intestinal organoids derived from human patients with UC can effectively recapitulate the
328 absence of goblet cells clinically observed in vivo (Extended Data Fig. 14 a and b). Therefore,
329 we established a UC organoid model based on intestinal epithelial cells isolated from the
330 mucosal layer of Chinese patients diagnosed with ulcerative colitis (Extended Data Fig. 15a).
331 During the organoid culture process, NALHP, S6, and 5-ASA were added to further investigate
332 the potential mechanism by which deanticoagulated HP contributes to the restoration of the
333 mucosal barrier in UC mice, as observed above (Fig. 2). Morphological analysis demonstrated
334 that NALHP and S6 significantly altered the three-dimensional structural features of the
335 organoids during culture (Fig. 3a1-a3, Extended Data Video 1): compared with those in the
336 control group, the organoids in the NALHP/S6 groups exhibited decreased sphericity (Fig. 3b)
337 and an increased surface density and smoothness. In contrast, no morphological alterations were
338 observed following culture with 5-ASA (Fig. 3a4). To characterize the cellular heterogeneity
339 among the groups of organoids, single-cell transcriptome profiling was conducted. The results
340 revealed that the percentage of LGR5+ stem cells and PCNA+ transient amplifying (TA) cells in
341 the UC organoid control group was greater than 90% (Fig. 3c, d and Extended Data Fig. 15b-e),
342 confirming the robust proliferative and differentiation capabilities—which are predominantly
343 stem cell-driven—of these UC patient-derived organoids, as reported previously[33]. While culture
344 with NALHP or S6 induced substantial remodeling of the cellular composition in the UC
345 organoids: the percentage of stem/TA cells decreased to less than 10%, whereas the percentage of
346 goblet progenitor cells and their mature subtypes was greater than 80%. Additionally,

347 approximately 5% of the intestinal epithelial cells exhibited markers of differentiation, indicating

348 that the culture of UC organoids with NALHP or S6 induced the development of a functionally

349 differentiated phenotype (Extended Data Fig. 15d and e), but no functionally differentiated

350 phenotype was detected in UC organoids cultured with 5-ASA (Fig. 3c and d).

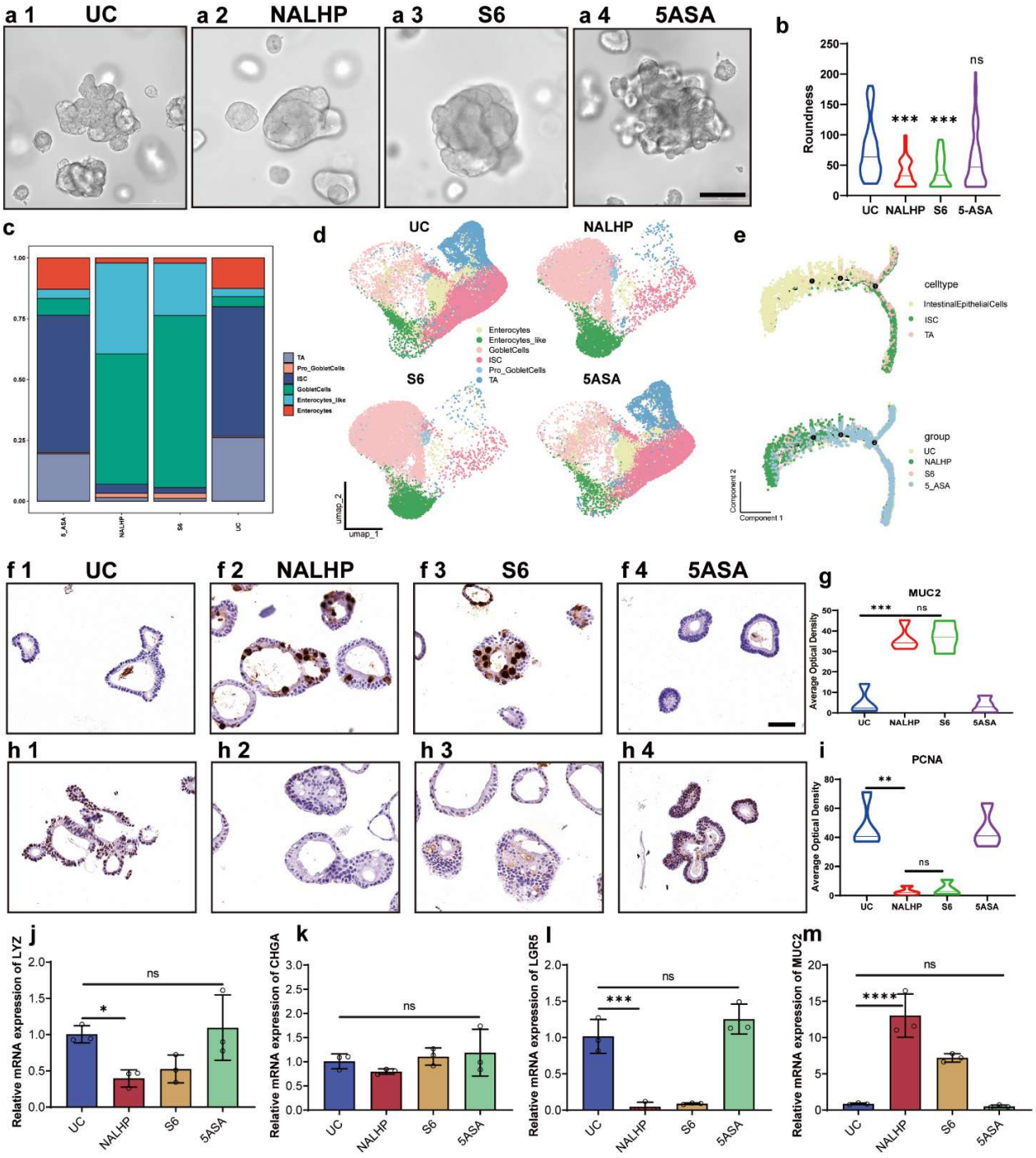

Fig. 3 NALHP and S6 promote the directed differentiation of goblet cells in organoids. a1–a4, Brightfield images of organoids. UC (a1), NALHP (a2), S6 (a3), and 5-ASA (a4) groups. **b,** Changes in the sphericity of the organoids. **c,** The percentages of cells in UC organoids in the

355 different groups. **d,** UMAP dimensionality reduction plot of UC organoids in the different

356 groups. **e,** Pseudotime analysis of UC organoids in the different groups and of cell types by

357 Monocle 2.**f1-f4.** Representative images of colons with hematoxylin and MUC2 staining and

358 quantitative immunohistochemical scores **(g)**. Scale bar, 50 μm. **h1-h4,** Representative images of

359 colons with hematoxylin and PCNA staining and quantitative immunohistochemical scores **(i)**.

360 Scale bar, 50 μm. **j–m,** Relative mRNA expression levels of LYZ **(j)**, CHGA **(k)**, LGR5 **(l)**, and

361 MUC2 **(m).**

362 Representative images or quantitative analysis results from n=3 biologically independent

363 samples are shown (**b, g, i, j-m**). The data are presented as the mean ± SD values. * $p < 0.05$, **

364 $p < 0.01$, *** $p < 0.001$, **** $p < 0.0001$ and ns (not significant) $p > 0.05$; the data were

365 analyzed by ordinary one-way ANOVA.

366 Furthermore, through the sequencing of temporal genes in the individual cells of UC organoids,

367 it was observed that organoids cultured with NALHP or S6 were composed of cells in the highly

368 differentiated stage, whereas the cells in the untreated group and in the group cultured with 5-

369 ASA remained in the early stage of differentiation (Extended Data Fig. 16a); moreover, the

370 highly differentiated cells were originated from the intestinal stem cell–TA cell hierarchy in the

371 organoids (Fig. 3e), leading to a marked increase in the abundance of mucus-secreting goblet

372 cells (Extended Data Fig. 16b). Considering this differentiation pattern, we examined the

373 transcription of secretory cell markers and detected no significant differences in the mRNA

374 expression levels of lysozyme (LYZ) and chromogranin A (CHGA) among the groups (Fig. 3j

375 and k). However, the mRNA expression level of MUC2 significantly increased, whereas the
376 mRNA expression level of LGR5 significantly decreased when the organoids were cultured with
377 NALHP or S6 (Fig. 3l and m). Based on these findings, we hypothesized that the primary
378 function of NALHP and S6 is to mediate the directed differentiation of intestinal stem cells
379 toward the goblet cell lineage. Immunohistochemical analysis further confirmed that the
380 fluorescence intensity of the MUC2 protein was more than tenfold greater in the NALHP/S6-
381 treated groups than in the control UC and 5-ASA-treated groups (Fig. 3f1-f4), while the PCNA
382 signal was correspondingly reduced (Fig. 3h1-h4). These findings were highly consistent with
383 the results of the single-cell transcriptomic analysis (Fig. 3c). Moreover, the above results were
384 verified in organoids derived from three patients (UC1-UC3) (Extended Data Figs. 15e and 17).
385 Taken together, these findings suggest that NALHP and S6 specifically promote the generation
386 of goblet cell lineages by activating the directed differentiation of intestinal stem cells in UC
387 organoids, thereby increasing the expression level of the mucin protein, similar to the effects
388 observed in UC mice (Fig. 2k4, k5, and Extended Data Fig. 13).
389 Interestingly, during the process of dissociating organoids into single cells by treatment with
390 pancreatic enzymes, we found that the organoids in the NALHP/S6 culture groups were more
391 resistant to dissociation into single cells, suggesting stronger connections between the cells in the
392 UC organoids cultured with NALHP or S6 than between those in the control UC organoids.
393 Next, we stimulated NCM460 cells, a kind of normal human colonic epithelial cell, with IL-6 to
394 reduce the strength of the connections between cells mediated by the ZO-1 junction protein cells

395 and found that treatment with NALHP or S6 reversed the IL-6-induced damage to this tight
396 junction protein connecting NCM460 cells (Extended Data Fig. 18). These findings also suggest
397 that NALHP and S6 may restore the tight junction proteins connecting stimulated colonic
398 epithelial cells.
399
400 ***NALHP & S6 drive stem cell differentiation to goblet cells in UC organoids via separate***
401 ***Wnt/Notch inhibition***
402 UC organoids from the groups cultured with various drugs (NALHP, S6 and 5-ASA) and the
403 control group were collected and subjected to transcriptome analysis. KEGG and GO enrichment
404 analyses of the differentially expressed genes in the organoids cultured with NALHP and S6
405 revealed significant enrichment of genes in the Wnt, Hippo, and Notch signaling pathways
406 (Extended Data Fig. 19a), which are key regulators of intestinal stem cell proliferation and
407 differentiation[33]. Given that Wnt and Notch are critically involved in the differentiation of
408 intestinal stem cells[34], modulating their activity enables precise control over the induction and
409 differentiation of various intestinal epithelial cell types, including goblet cells. Both NALHP and
410 S6 promoted the differentiation of intestinal stem cells into goblet cells (Fig. 3j and m).
411 Furthermore, when the UC organoids were cultured with the combination of the Wnt pathway
412 inhibitor IWP-2 and the Notch pathway inhibitor DAPT, the percentage of goblet cells within the
413 organoids increased to more than 60% (Extended Data Fig. 19b-e), which is consistent with the
414 mediation effects observed upon culture with NALHP or S6. To validate the central role of Wnt

415 and Notch pathway inhibition in NALHP/S6-mediated differentiation, functional rescue
416 experiments were conducted using CHIR99021 (C), a Wnt pathway agonist, and sodium
417 valproate (VPA, V), a Notch pathway agonist. In the presence of these agonists, the ability of
418 NALHP and S6 to promote the differentiation of intestinal stem cells (marked by LGR5) into
419 goblet cells (marked by MUC2) was partially abolished: UC organoid budding morphology was
420 restored (Extended Data Fig. 20), and the expression levels of Wnt- and Notch-related proteins,
421 whose expression was previously suppressed by NALHP/S6 treatment, were restored. Coculture
422 with the agonists significantly restored LGR5 expression and reduced MUC2 mRNA expression
423 ($p < 0.001$) in UC organoids (Fig. 4a and b). Additionally, the transcription and translation of
424 TCF1, a downstream effector of the Wnt pathway, were markedly inhibited in the agonist-treated
425 UC organoids (Fig. 4c and f). These findings clearly indicate that dual inhibition of the Wnt and
426 Notch pathways in UC organoids constitutes the primary mechanism underlying the biological
427 activity of NALHP/S6 in mediating the differentiation of goblet cells to increase the secretion of
428 mucosal layer components.

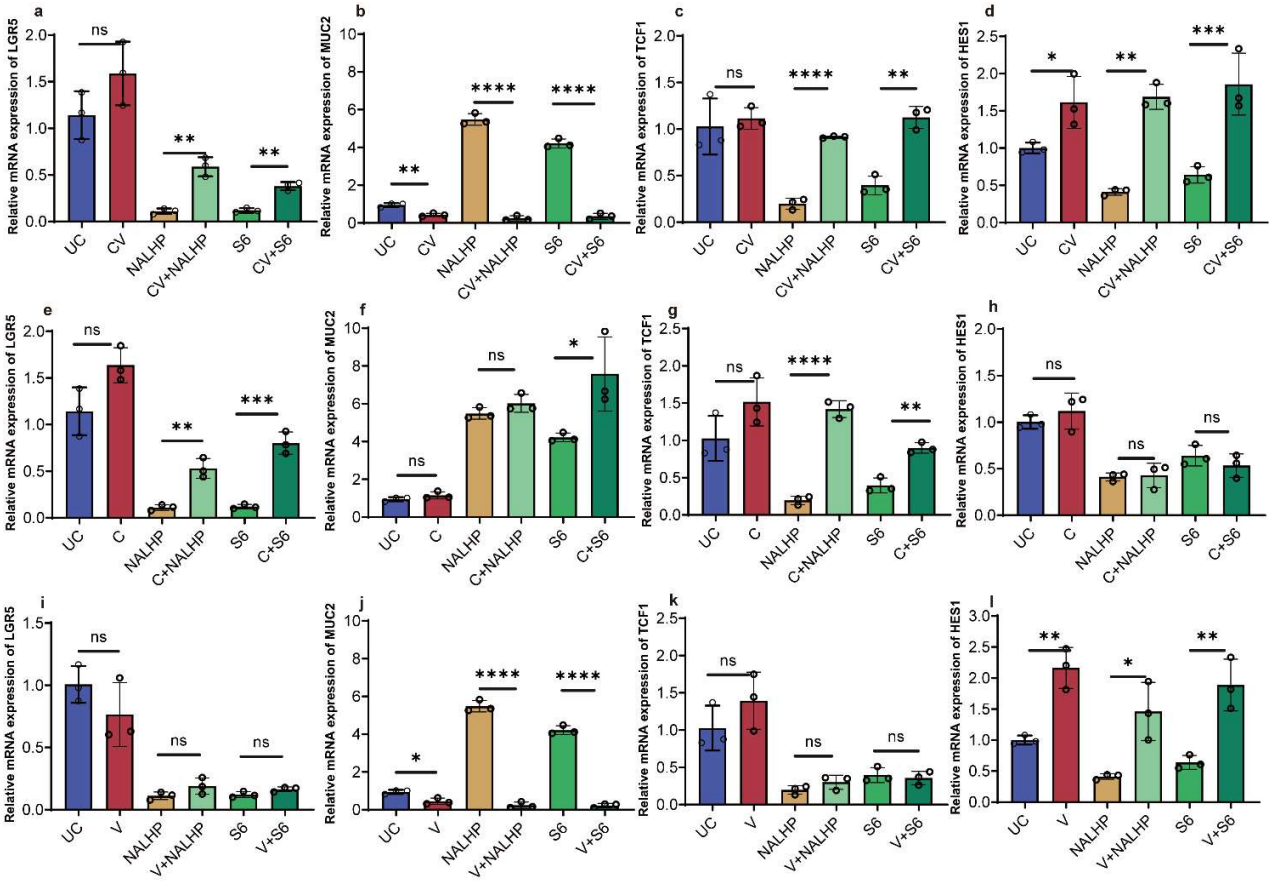

429

430 **Fig. 4 Changes in UC organoids upon treatment with different inhibitors. a–d,** The relative

431 mRNA expression levels of LGR5 (**a**), MUC2 (**b**), TCF1 (**c**), and HES1 (**d**) in UC organoids

432 after treatment with CHIR99021 (C), VPA (V) and NALHP/S6. **e-h,** The relative mRNA

433 expression levels of LGR5 (**e**), MUC2 (**f**), TCF1 (**g**), and HES1 (**h**) in UC organoids after

434 treatment with CHIR99021 (C) and NALHP or S6. **i–l,** The relative mRNA expression levels of

435 LGR5 (**i**), MUC2 (**j**), TCF1 (**k**), and HES1 (**l**) in UC organoids after treatment with VPA (V) and

436 NALHP or S6.

437 Representative results of the quantitative analysis of n=3 biologically independent samples are

438 shown (**a–l**). The data are presented as the mean ± SD values. * $p < 0.05$, ** $p < 0.01$, *** $p <$

439 0.001, **** $p < 0.0001$ and ns (not significant) $p > 0.05$; the data were analyzed by ordinary one-
440 way ANOVA.
441 During the development of the intestinal tract, Wnt and Notch signaling can determine the fate of
442 intestinal stem cells. We selected the downstream effectors TCF1 and HES1, which are related to
443 the Wnt and Notch signaling pathways, to further determine the influence of these pathways. The
444 expression level of HES1 during the development of goblet cells is highly important. High
445 expression levels of HES1 inhibit the process of differentiation toward goblet cells. Culture with
446 NALHP or S6 led to significant inhibition of Hes1 and TCF1 mRNA expression (Fig. 4c and d),
447 and agonist treatment partially reversed this effect, with a consistent effect at the translational
448 level (Extended Data Fig. 21). To determine the individual contributions of each pathway,
449 CHIR99021 and VPA were applied separately in combination with NALHP or S6. Gene
450 expression analysis revealed that CHIR99021 restored LGR5 mRNA expression (indicative of
451 stemness) (Fig. 4e) and activated the Wnt signaling pathway (Fig. 4g and Extended Data Fig. 22)
452 but did not inhibit the upregulation of MUC2 (Fig. 4f) or regulate the Notch signaling pathway
453 (Fig. 4h). Conversely, VPA suppressed the induction of MUC2 expression by activating the
454 Notch signaling pathway (Fig. 4j, m and Extended Data Fig. 23), but it did not regulate the Wnt
455 signaling pathway (Fig. 4k) to restore the expression of LGR5 (Fig. 4i). Collectively, these
456 results demonstrate that NALHP and S6 exert their effects by coordinately modulating both the
457 Wnt and Notch pathways to drive the directed differentiation of intestinal stem cells into goblet
458 cells.

459 **Discussion**

460 The absence of a mucus layer and the impairment of the intestinal epithelial barrier—
461 pathological features whose complexity imposes stringent demands on existing therapeutic
462 agents—are the central challenges in UC treatment[35]. In the development of anti-UC
463 medications, HP, a classic anticoagulant drug, has demonstrated potential in alleviating intestinal
464 inflammation. However, the data from nearly three decades of trial-and-error studies reveal
465 substantial variability and even contradictory outcomes regarding its efficacy; these limitations
466 are compounded by the inherent hemorrhagic risks of these drugs, preventing the in-depth and
467 broad exploration of their nonanticoagulant activity. In this study, we innovatively propose the
468 critical hypothesis that the anticoagulant activity of HP enriched during drug production may
469 interfere with its anti-UC activity. By employing the strong oxidation performance of sodium
470 periodate to open the ring of glucuronic acid, one of the anticoagulant pentasaccharides[3], the
471 ability of sodium borohydride reduction to stabilize the open ring structure, and subsequent
472 depolymerization by heparinase I[3], we obtained a novel deanticoagulated HP derivates, NALHP,
473 which has no anticoagulant activity, but does exhibit stable and effective anti-UC activity (Fig.
474 1a, Extended Data Figs. 2 and 3).

475 The interference of anticoagulant activity enriched during heparin drug manufacturing is one of
476 the reasons that the nonanticoagulant activity of conventional heparin drugs is difficult to
477 explore. We have adopted various methods to prepare heparin derivates without anticoagulant
478 activity. The derivate III,II-2-Odes-1, which does not contain sulfonate groups, did not exhibit

479 significant therapeutic activity against UC. The derivates NAHP, obtained by opening the ring
480 with potassium periodate, exhibited obvious therapeutic activity against UC, indicating that
481 sulfonation is one of the key factors for the ability of heparin to treat UC. Chemical degradation
482 of Eno and NAEno did not result in a therapeutic effect on UC, indicating that chemical
483 degradation for production of Eno destroys the active anti-UC fragments. Molecular weight is
484 also a key factor for the release of heparin activity. Therefore, we used our previously established
485 heparinase expression system and expressed heparinases I, II, and III. Using the recombinant
486 heparinases, we controlled the reduction in the molecular weight of NAHP to obtain NALHP,
487 NAULHP and 11 fine separation fragments from the NALHP (Fig.1b, Extended Data Table.1).
488 The reduction in molecular weight increased the therapeutic activity against UC, but NALHP
489 treatment resulted in a higher survival rate in UC mice. In addition, among the 11 separated
490 fragments, the efficacy of S6 is consistent with that of NALHP, the efficacy of S4 is like that of
491 NAULHP, and S10 shows no significant efficacy, indicating that an appropriate molecular
492 weight (3000Da-8000Da) is another key factor for the ability of deanticoagulated HP to treat UC
493 (Extended Data Fig. 4j, Extended Data Table.1). The unique structural modification of the
494 anticoagulant pentasaccharide domain[3] in NALHP not only eliminated the anticoagulant
495 properties of HP but also resulted in anti-UC activity. The formation of gsGlcA results from
496 redox reaction-induced ring opening of glucuronic acid residues, whereas Δ4,5-unsaturated
497 glucuronic acid is a characteristic product generated during the heparinase I-mediated cleavage
498 of glycosidic bonds (Fig. 1e-g and Extended Data Fig. 5).

499 The primary structural differences between HP and NALHP are the presence and absence,
500 respectively, of the active anticoagulant pentasaccharide sequence and variations in the
501 molecular weight distribution. Thus, this unique preparation process enabled the discovery of the
502 unique therapeutic mechanism of deanticoagulated HP derivates in UC. NALHP has a broad
503 molecular weight distribution (PDI=2.23). After separation by gel chromatography, fragment S6,
504 with a molecular weight within the range of 3000Da to 5000Da and a PDI of 1.1 and accounting
505 for 15.3% (w/w) of the content of NALHP (Extended Data Table 1 and Fig. 1b), had the same or
506 an even greater therapeutic effect in UC relative to NALHP (Fig. 2). We also attempted to change
507 the order of preparation of the deanticoagulation by sodium borohydride reduction and
508 enzymatic depolymerization of HP and found that NAI45, a product generated by an initial
509 enzymatic reaction resulting in a low molecular weight followed by a reaction resulting in the
510 loss of anticoagulant property[3], did not exhibit therapeutic activity against UC (Extended Data
511 Fig. 4), indicating that the unique preparation route is also one of the reasons that the different
512 structure of NALHP allows it to exert therapeutic effects on UC (Extended Data Figs. 2 and 4).
513 In addition, we cocultured organoids with fondaparinux sodium and nonanticoagulant
514 fondaparinux sodium but found that it did not have the same effect as NALHP did (Extended
515 Data Fig. 24). These results indicate that the intestinal stem cell differentiation-promoting
516 activity and anticoagulant activity are independent in HP molecules.
517 To elucidate how NALHP/S6 alleviate UC, comprehensive in vitro and in vivo experiments
518 using UC mice were conducted. Initial observations indicated that oral NALHP administration

519 reduced inflammatory cell infiltration in colonic crypts, decreased serum inflammatory cytokine
520 concentrations, and restored the orderly proliferation of damaged crypt structures in UC mice,
521 effects that collectively ameliorated UC pathology (Fig. 2). Subsequent multiomics analysis
522 revealed that the mechanism underlying the effects of NALHP in UC mice is dependent on
523 intestinal epithelial wound healing and stem cell proliferation/differentiation (Extended Data
524 Figs. 10 and 11). Further validation using a human patient-derived UC organoid model revealed
525 that NALHP/S6 restored the differentiation trajectory of LGR5+ stem cells, in turn increasing the
526 proportion of mucus-secreting goblet cells in UC organoids from <10% to ≥80% (Fig. 3c), which
527 was consistent with the findings in the mouse model (Extended Data Figs. 11-13). This unique
528 differentiation-promoting mechanism effectively repaired colonic crypt structural units,
529 reestablishing the dual protection offered by the intestinal mechanical and chemical barriers. The
530 Wnt and Notch signaling pathways are crucial factors determining the fate of intestinal crypt
531 stem cells[34]. NALHP and S6 inhibited the Wnt and Notch signaling pathways in UC organoids,
532 and their effects were consistent with those of IWP-2 and DAPT (Extended Data Fig. 19). On the
533 other hand, adding CHIR99021 and VPA could re-activate the Wnt and Notch signaling
534 pathways that were inhibited by NALHP and S6, the proliferation and differentiation levels of
535 intestinal stem cells have been returned (Fig. 4, Extended Data Fig. 20 and Extended Data
536 Videos 1-6). These findings indicate that NALHP/S6 not only alleviates UC by inhibiting
537 inflammatory responses, as do 5-ASA[36] and infliximab, but also specifically promotes the repair
538 of the mucosal layer barrier in UC.

539 As all intestinal crypt cells originate from LGR5+ stem cells at the crypt base, crypt destruction
540 contributes to the refractory nature of UC[37-39]. Endoscopic mucosal healing is considered the
541 gold standard for the success of clinical UC therapy. Using UC mice model and human patient-
542 derived UC organoid model, we proved that NALHP/S6 promoted goblet cell differentiation in
543 the mucus layer, reduced the abnormal proliferation of intestinal stem cells and reinforced the
544 crypt self-renewal capacity by regulating the Wnt and Notch signaling pathways (Fig. 4 and
545 Extended Data Fig. 19), thereby repairing the intestinal mucosal barrier. In this article, we
546 present stably prepared deanticoagulated HP derivates, which overcomes the difficulty that
547 anticoagulant HP is unable to provide stable treatment for UC. This study demonstrates for the
548 first time that the deanticoagulated HP derivates NALHP and S6 exert mucosal barrier repair
549 effects by regulating crypt stem cell fate, offering an innovative strategy to overcome the
550 limitations of current drugs in UC therapy. The successful development of NALHP provides a
551 promising strategy for identifying the pleiotropic UC-treatment mechanisms of nonanticoagulant
552 heparin drugs, which has substantial translation value.
553

References

1. Villablanca, E. J., Selin, K. & Hedin, C. R. H. Mechanisms of mucosal healing: treating inflammatory bowel disease without immunosuppression? *Nat. Rev. Gastroenterol. Hepatol.* **19**, 493–507 (2022).
2. Alsoud, D., Verstockt, B., Fiocchi, C. & Vermeire, S. Breaking the therapeutic ceiling in drug development in ulcerative colitis. *Lancet Gastroenterol. Hepatol.* **6**, 589–595 (2021).
3. Ji, Y. et al. A heparin derivates library constructed by chemical modification and enzymatic depolymerization for exploitation of non-anticoagulant functions. *Carbohydr. Polym.* **249**, 116284 (2020).
4. Feuerstein, J. D. et al. AGA clinical practice guidelines on the management of moderate to severe ulcerative colitis. *Gastroenterology* **158**, 1450–1463 (2020).
5. Ulcerative colitis. *Journal* **6**, 73 (2020).
6. Alatab, S. et al. The global, regional, and national burden of inflammatory bowel disease in 195 countries and territories, 1990-2017: a systematic analysis for the Global Burden of Disease Study 2017. *Lancet Gastroenterol. Hepatol.* **5**, 17–30 (2020).
7. Gajendran, M. et al. A comprehensive review and update on ulcerative colitis. *Dis. Mon.* **65**, 100851 (2019).
8. Abraham, C. & Cho, J. H. Inflammatory bowel disease. *N. Engl. J. Med.* **361**, 2066–2078 (2009).

9. Beaugerie, L. & Itzkowitz, S. H. Cancers complicating inflammatory bowel disease reply. *N. Engl. J. Med.* **373**, 195–195 (2015).

10. Nakase, H. et al. Evidence-based clinical practice guidelines for inflammatory bowel disease 2020. *J. Gastroenterol.* **56**, 489–526 (2021).

11. Singh, S., Murad, M. H., Fumery, M., Dulai, P. S. & Sandborn, W. J. First- and second-line pharmacotherapies for patients with moderate to severely active ulcerative colitis: an updated network meta-analysis. *Clin. Gastroenterol. Hepatol.* **18**, 2179–2191.e6 (2020).

12. Mowat, C. et al. Guidelines for the management of inflammatory bowel disease in adults. *Gut* **60**, 571–607 (2011).

13. Peyrin-Biroulet, L. & Lémann, M. Review article: remission rates achievable by current therapies for inflammatory bowel disease. *Aliment. Pharmacol. Ther.* **33**, 870–879 (2011).

14. Okayasu, M., Ogata, H. & Yoshiyama, Y. Use of corticosteroids for remission induction therapy in patients with new-onset ulcerative colitis in real-world settings. *J. Mark. Access Health Policy* **7**, 1565889 (2019).

15. Kayal, M. & Shah, S. Ulcerative colitis: current and emerging treatment strategies. *J. Clin. Med.* **9**, 12 (2020).

16. Bhattacharya, A. & Osterman, M. T. Biologic therapy for ulcerative colitis. *Gastroenterol. Clin. N. Am.* **49**, 717–729 (2020).

17. Hirten, R. P. & Sands, B. E. New therapeutics for ulcerative colitis in *Annual Review of*

Medicine (ed M. E. Klotman) 199–213 (Annual Reviews, 2021).

18. Mulloy, B., Hogwood, J., Gray, E., Lever, R. & Page, C. P. Pharmacology of heparin and related drugs. *Pharmacol. Rev.* **68**, 76–141 (2016).

19. Oduah, E. I., Linhardt, R. J. & Sharfstein, S. T. Heparin: past, present, and future. *Pharmaceuticals (Basel, Switzerland)* **9**, 38 (2016).

20. Cui, J. et al. Highly sensitive and selective detection of heparin in serum based on a long-wavelength tetraphenylethylene-cyanopyridine aggregation-induced emission luminogen. *Anal. Chem.* **92**, 7106–7113 (2020).

21. Gray, E., Hogwood, J. & Mulloy, B. The anticoagulant and antithrombotic mechanisms of heparin in *Heparin - A Century of Progress. Handbook of Experimental Pharmacology* (eds R. Lever, B. Mulloy, & C. Page) 43–61 (Springer, 2012).

22. Ang, Y. S. et al. Randomized comparison of unfractionated heparin with corticosteroids in severe active inflammatory bowel disease. *Aliment. Pharmacol. Ther.* **14**, 1015–1022 (2000).

23. Ludwig, R. J. et al. The ability of different forms of heparins to suppress P-selectin function in vitro correlates to their inhibitory capacity on bloodborne metastasis in vivo. *Thromb. Haemost.* **95**, 535–540 (2006).

24. Kim, S. Y. et al. Glycosaminoglycan compositional analysis of relevant tissues in Zika virus pathogenesis and in vitro evaluation of Heparin as an antiviral against Zika virus infection. *Biochemistry* **58**, 1155–1166 (2019).

614 25. Gaffney, P. R. et al. Paradoxical response to heparin in 10 patients with ulcerative-colitis.
615 *Am. J. Gastroenterol.* **90**, 220–223 (1995).
616 26. Törkvist, L. et al. Low molecular weight heparin as adjuvant therapy in active ulcerative
617 colitis. *Aliment. Pharmacol. Ther.* **13**, 1323–1328 (1999).
618 27. Zezos, P. et al. Low-molecular-weight heparin (enoxaparin) as adjuvant therapy in the
619 treatment of active ulcerative colitis: a randomized, controlled, comparative study.
620 *Aliment. Pharmacol. Ther.* **23**, 1443–1453 (2006).
621 28. Chande, N., MacDonald, J. K., Wang, J. J. & McDonald, J. W. D. Unfractionated or low
622 molecular weight heparin for induction of remission in ulcerative colitis: a cochrane
623 inflammatory bowel disease and functional bowel disorders systematic review of
624 randomized trials. *Inflamm. Bowel Dis.* **17**, 1979–1986 (2011).
625 29. Huang, L. et al. "Two-birds-one-stone" oral nanotherapeutic designed to target intestinal
626 integrins and regulate redox homeostasis for UC treatment. *Sci. Adv.* **10**, eado7438
627 (2024).
628 30. Darwish, N. H. E., Godugu, K. & Mousa, S. A. Sulfated non-anticoagulant low molecular
629 weight heparin in the prevention of cancer and non-cancer associated thrombosis without
630 compromising hemostasis. *Thromb. Res.* **200**, 109–114 (2021).
631 31. Hirano, A. et al. Comparison of the microbial community structure between inflamed and
632 non-inflamed sites in patients with ulcerative colitis. *J. Gastroenterol. Hepatol.* (2018).
633 32. Zhao, X. et al. Porphyromonas gingivalis exacerbates ulcerative colitis via

634 Porphyromonas gingivalis peptidylarginine deiminase. *Int. J. Oral Sci.* **13**, 31 (2021).

635 33. Malagola, E. et al. Isthmus progenitor cells contribute to homeostatic cellular turnover
636 and support regeneration following intestinal injury. *Cell* **187**, 3056–3071.e17 (2024).

637 34. Yin, X. et al. Niche-independent high-purity cultures of Lgr5+ intestinal stem cells and
638 their progeny. *Nat. Methods* **11**, 106–112 (2014).

639 35. Hirten, R. P. & Sands, B. E. New therapeutics for ulcerative colitis. *Annu. Rev. Med.* **72**,
640 199–213 (2021).

641 36. Tang, S. et al. Sustained release of 5-aminosalicylic acid from azoreductase-responsive
642 polymeric prodrugs for prolonged colon-targeted colitis therapy. *J. Nanobiotechnology*
643 **22**, 468 (2024).

644 37. Schlegel, N. Promoting mucosal healing by targeting TMEM219-dependent intestinal
645 epithelial stem cell defects in inflammatory bowel disease. *J. Clin. Invest.* **135**, e192640
646 (2025).

647 38. Sarvestani, S. K. et al. Induced organoids derived from patients with ulcerative colitis
648 recapitulate colitic reactivity. *Nat. Commun.* **12**, 262 (2021).

649 39. Wu, J. et al. EFHD2 suppresses intestinal inflammation by blocking intestinal epithelial
650 cell TNFR1 internalization and cell death. *Nat. Commun.* **15**, 1282 (2024).

651 **Methods**

652

653 ***Preparation of deanticoagulated HP derivates***[3]

654 The preparation process of deanticoagulated HP derivates was described previously. Briefly,
655 pharmaceutical-grade HP sodium was purchased from Changshan Biochemical Pharmaceutical
656 Co., Ltd. (Hebei, China). To eliminate anticoagulant activity, HP was dissolved in water at a
657 concentration of 33 mg/ml. The solution was reacted with an equal volume of 0.2 M periodate
658 sodium solution at 4 °C for 22 hr prior to neutralization reactions with 4 ml of glycol and 1.4 g of
659 sodium borohydride per gram of HP at 4 °C for 1 hr and 16 hr, respectively. The resulting
660 solution was adjusted to pH 7.0, filtered through a membrane, desalted using a 3 kDa Pellicon 2
661 Mini Cassette (Millipore, Germany), and lyophilized to obtain nonanticoagulated HP (NAHP).
662 NAHP was subsequently subjected to further enzymolysis with recommbinant heparinase I
663 (Beijing Bio-Cell Technology Co., Ltd., China). NAHP was dissolved in a reaction buffer
664 consisting of 20 mM Tris, 200 mM NaCl, and 5 mM $CaCl_2$ at pH 7.4. The increase in the
665 absorbance at 232 nm was recorded immediately after the heparinase I was added to the NAHP
666 solution. Low-molecular-weight NAHP (NALHP) and ultra-low-molecular-weight NAHP
667 (NAULHP) were obtained when the absorbance increased to 45 and 100, respectively. The
668 excess heparinase I was inactivated once the increase reached the endpoint by heating the
669 solution at 100 °C for 10 min. The solution was filtered, precipitated with alcohol, and
670 lyophilized to obtain NALHP and NAULHP. The HP derivates NAI45 was prepared through the

671 enzymolysis of HP using the heparinase I, allowing the increase in the absorbance to reach 45,
672 followed by periodate sodium oxidation and sodium borohydride reduction. The
673 deanticoagulated enoxaparin (NAEno) was prepared from commercial enoxaparin (Changshan
674 Biochemical Pharmaceutical Co., Ltd., Hebei, China) using the same preparation process used
675 for the oxidation of HP to NAHP.
676
677 ***Molecular Weight Determination Of Deanticoagulated HP Derivates***
678 The molecular weight of each HP derivates was determined using gel penetration
679 chromatography (GPC) as described previously. In short, an HPLC system (Waters, America)
680 with a binary pump module, an autosampler, and a refractive index detector was used. The
681 mobile phase consisted of 0.2 M sodium sulfate solution at pH 5.0. HP derivates, the HP sodium
682 molecular weight calibrant (USP, America), and low-molecular-weight HP for molecular weight
683 calibration (NIBSC, America) were dissolved in the mobile phase at a concentration of 20
684 mg/ml. The samples were subsequently injected onto a 300 × 7.8-mm TSK Gel G2000SW$_{XL}$
685 column (Tosoh, Japan) in a volume of 25 μl. The column was eluted at a flow rate of 0.5 ml/min
686 and a temperature of 35 °C. The data were collected and analyzed in Breeze 2 (Waters, America)
687 software. The molecular weight distributions of the HP derivates were calculated based on the
688 standard curve generated from the calibrant with a general third-order calibration method.
689
690 ***Fine separation of the NALHP***

691 Fine separation of the HP derivates was performed using a HiPrep 16/60 Sephacryl S-100 HR
692 column (GE Healthcare, America) with a ÄKTA prime purification system (GE Healthcare,
693 America). The mobile phase consisted of 0.2 M sodium chloride solution at pH 5.0. The HP
694 derivates NALHP was dissolved in the mobile phase at a concentration of 120 mg/ml. The
695 sample was subsequently injected onto the column using a 5 ml injection loop. The column was
696 eluted at a flow rate of 0.5 ml/min at room temperature. Fractions were collected every 10 min
697 from 70 min to 180 min after sample injection and were designated S1 to S11 according to the
698 order of retention time. Afterward, the samples were lyophilized and reconstituted in water at
699 30% of the original volume to enrich polysaccharides, and alcohol precipitation and another
700 lyophilization step were then performed to obtain the separated components.
701
702 ***Mouse model of DSS-induced colitis***
703 Male C57BL/6J mice (18–22 g, 6–8 weeks) were purchased from Vital River Laboratories
704 (Beijing, China). The mice were housed under specific pathogen-free conditions in the laboratory
705 animal facility of Tsinghua University. The animal protocols 17-XXH1 and 20-XXH1 were
706 carried out with the approval of the Institutional Animal Care and Use Committee (IACUC) of
707 Tsinghua University. The laboratory animal facility was accredited by AAALAC (Association
708 for Assessment and Accreditation of Laboratory Animal Care) International.
709 Evaluation of the anti-UC efficacy of the HP derivates was performed using a 7-day mouse
710 model of acute colitis. All the mice were pre-fed for one week prior to any subsequent

711 experiments. The mice were given 3% DSS (dextran sulfate sodium; colitis grade, MP
712 Biomedicals, America) solution instead of water for 7 consecutive days. The HP derivates and 5-
713 aminosalicylic acid (5-ASA) were dissolved in saline at a concentration of 3 mg/ml. Starting 3
714 days post-DSS induction, the mice were orally administered the drug solution daily at a dosage
715 of 30 mg/kg/d. The mice were euthanized by CO_2 inhalation after DSS induction for 7 days. The
716 serum was separated from the cardiac blood of the mice, while the spleens and the colons were
717 excised and measured. The colon tissue was cut in the longitudinal direction, washed with ice-
718 cold PBS, rolled with the Swiss-rolling technique, fixed, and embedded in paraffin for further
719 investigations.
720 Multiomics analyses were performed in a 14-day mouse colitis model to evaluate the systemic
721 changes in mice with colitis caused by drugs. The mice were allowed to drink 3% DSS solution
722 for 3 days, after which they received standard drinking water and drug treatment for 4 days.
723 Afterward, the mice were allowed to drink 2% DSS solution for another 3 days, after which they
724 received standard drinking water and drug treatment for another 4 days. Fresh feces were
725 collected prior to euthanasia by CO_2 inhalation. After the mice were sacrificed, the colons were
726 removed. The colonic contents were collected while the colonic epithelial tissue was scraped and
727 collected in 1.5 ml centrifuge tubes containing TRIzol reagent (Invitrogen, America).
728
729 ***ELISA***
730 The concentrations of interleukin-6 (IL-6) and tumor necrosis factor-alpha (TNF-α) in serum and

731 cell culture medium were measured using an IL-6 Mouse ELISA Kit (Invitrogen, America) and a
732 TNF-α Mouse ELISA Kit (Invitrogen, America), respectively, according to the manufacturer's
733 instructions.
734
735 ***Biolayer interferometry***
736 The molecular interactions between DSS and the HP derivates were evaluated using an Octet
737 Red96 instrument (FortéBIO, America). DSS and the HP derivates were dissolved in HBS-EP
738 buffer containing 10 mM HEPES, 150 mM NaCl, 3 mM EDTA, and 0.005% Tween 20 at pH
739 7.4. The streptavidin sensors were loaded with DSS washed in HEB-EP buffer and exposed to
740 the HP derivates.
741
742 ***RNA isolation and qPCR***
743 Total RNA was extracted using TRIzol reagent (Invitrogen) and reverse transcribed to cDNA
744 using a FastKing RT Kit (TIANGEN, China). All qPCRs were run in a CFX96 Touch Real-Time
745 PCR Detection System (Bio-Rad, America) using Talent qPCR PreMix (TIANGEN, China) with
746 the specific primers listed in the extended data.
747
748 ***FTIR spectroscopy***
749 The infrared absorption spectra of the HP derivates were generated using a Nicolet 6700 FTIR
750 spectrometer (Thermo Electron Corporation, Shanghai, China) with the potassium bromide tablet

751 method. The spectral data were collected in a 4000–400 cm^{-1} range for all the samples.

752

753 ***NMR analysis***

754 For 1D (^{1}H, ^{13}C) and 2D-NMR analyses, HP derivates (50–60 mg) were dissolved in 0.6 mL of

755 deuterium oxide and lyophilized repeatedly to remove exchangeable protons. The thoroughly

756 dried samples were then dissolved in 0.5 mL of deuterium oxide with 0.002% 3-(trimethylsilyl)

757 propionate sodium salt (TSP) and transferred into 25 × 0.5-cm NMR tubes (Wilmad Lab Glass,

758 America). 1D (^{1}H, ^{13}C) and 2D-NMR experiments were performed at 298 K on a Bruker

759 Advance 600 MHz spectrometer (Germany) equipped with a 5 mm helium-cooled cryoprobe

760 using the following parameters: Proton—number of scans, 16; number of dummy scans, 2;

761 relaxation delay, 1.0 s; spectral width, 20 ppm; and transmitter offset, 6.0 ppm. One-dimensional

762 ^{13}C spectra were obtained with proton decoupling during acquisition at 298 K over 5000 scans.

763 All the spectra were Fourier transformed, phased and baseline corrected. The chemical shift

764 values were calibrated with TSP at 0.00 ppm. HSQC spectra were recorded with carbon

765 decoupling during acquisition with 256 increments of 16 scans. The polarization transfer delay

766 was set for a $^{1}J_{C\text{-}H}$ coupling value of 145 Hz.

767

768 ***Microbiome analysis***

769

770 *Sample preparation and DNA extraction*

771 Fresh fecal samples from UC mice were collected in 1.5-ml centrifuge tubes and stored
772 immediately at –80 °C until further analysis. Microbial genomic DNA samples were extracted
773 using a DNeasy PowerSoil Kit (QIAGEN, Germany) following the manufacturer's instructions.
774 The DNA concentrations in the samples were subsequently quantified using a NanoDrop ND-
775 1000 spectrophotometer (Thermo Fisher Scientific, America), and the samples were then
776 qualified by agarose gel electrophoresis.
777
778 *16S rRNA amplicon sequencing*
779 The V3–V4 region of the bacterial 16S rRNA gene was amplified by PCR using the forward
780 primer 338F (5'-ACTCCTACGGGAGGCAGCA-3') and the reverse primer 806R (5'-
781 CGGACTACHVGGGTWTCTAAT-3'). Sample-specific 7-bp barcodes were added to the
782 primers for further multiplex sequencing. PCR amplicons were purified using VAHTS^{TM} DNA
783 Clean Beads (Vazyme, China) and quantified using a PicoGreen dsDNA Assay Kit (Invitrogen,
784 America) prior to manipulation to achieve equal amounts of DNA. Afterward, paired-end 2 ×
785 250 bp sequencing was performed on the MiSeq platform (Illumina, America) with a NovaSeq
786 6000 SP Reagent Kit.
787
788 *Microbiome data analysis*
789 The raw sequence data were processed with QIIME2 2019.4 (Bolyen *et al*. 2018) with slight
790 modifications based on the official tutorials (https://docs.qiime2.org/2019.4/tutorials/). In brief,

791 the raw data were demultiplexed with the demux plugin, and primers were removed with the cut
792 adapt plugin. Afterward, the data were subjected to quality filtering, denoising, merging, and
793 chimera removal with the DADA2 plugin. A count table without rarefaction was used for further
794 analysis. The following analysis was carried out using an in-house-developed R script in Rstudio
795 software (v.2021.09.1, R version 4.1.2). Alpha diversity analysis and principal coordinate
796 analysis (PcoA) were performed using the vegan (v.2.5-7) package. Enterotyping was performed
797 with the Dirichlet multinomial mixture model with the DirichletMultinomial (v.1.36.0) package.
798 Data visualization was performed using the ggplot2 (v.3.3.5) and ggalluvial (v.0.12.3) packages.
799 In addition, LefSe analysis was performed on the Genescloud platform
800 (https://www.genescloud.cn/home).
801
802 ***Metabolome analysis***
803
804 *Sample preparation and extraction*
805 Samples of the colonic contents were thawed on ice. Aqueous homogenates were obtained by
806 mixing 100 mg of each sample with 300 μl of ice-cold water and steel balls for 5 min prior to
807 incubation on ice for 10 min. Then, 500 μl of methanol was added, and the homogenates were
808 mixed by vortexing for 5 min prior to incubation on ice for another 10 min. The homogenates
809 were centrifuged (12,000 rpm, 4 °C, 10 min), and 600 μl of the supernatant was transferred to
810 1.5-ml centrifuge tubes for further concentration. The concentrated dry products were dissolved

811 in 100 μl of 5% methanol–water, vortexed, and centrifuged (12,000 rpm, 4 °C, 10 min). Finally,
812 the supernatants were collected for LC–MS/MS analysis.
813
814 *LC–MS analysis*
815 A combination of positive ion mode MS and negative ion mode MS was applied to identify the
816 metabolites in the colonic contents. Data were acquired with an LC–MS system comprising a
817 1290 Infinity LC System (Agilent, America) coupled to a 6545 LC/Q-TOF mass spectrometer
818 (Agilent, America). The method details are summarized as follows. The supernatants were
819 injected onto a 100 × 2.1-mm ACQUITY UPLC HSS T3 C18 column (Waters, America) in a
820 volume of 2 μl. The column was eluted at a flow rate of 400 μl/min and a temperature of 40 °C.
821 Mobile phase A (water with 0.1% formic acid) and mobile phase B (acetonitrile with 0.1%
822 formic acid) were used with the following gradient program: 95:5 V/V A:B at 0 min, 10:90 V/V
823 at 11.0 min, 10:90 V/V at 12.0 min, 95:5 V/V at 12.1 min, 95:5 V/V at 14.0 min. In positive ion
824 mode, MS analysis was carried out using the following settings: ion spray voltage, 250; gas flow,
825 8; fragmentor, 135; gas temperature, 325 °C; sheath temperature, 325 °C; sheath flow, 11; and
826 nebulizer, 40. In negative ion mode, MS analysis was carried out using the following settings:
827 ion spray voltage, 1,500; gas flow, 8; fragmentor, 135; gas temperature, 325 °C; sheath
828 temperature, 325 °C; sheath flow, 11; nebulizer, 40.
829
830 *Metabolome data analysis*

831 The raw data obtained by LC–MS analysis were first converted into mzML format with
832 ProteoWizard software. Peak extraction, alignment, and retention time correction were carried
833 out with the XCMS program, while the peak area was corrected using the “SVR” method. Peaks
834 with a deletion rate of > 50% were filtered out in each group of samples. Next, metabolic
835 identification information was obtained by searching the laboratory’s in-house-built database and
836 integrating the public database and the metDNA tool. Finally, statistical analysis was carried out
837 using an in-house-developed R script in RStudio software (v.2021.09.1, R version 4.1.2).
838 Metabolites at the MS2 confidence level were selected for the following analysis. Principal
839 component analysis (PCA) was performed and the results were visualized using the vegan
840 (v.2.5–7) and ggplot2 (v.3.3.5) packages, respectively. Orthogonal partial least squares
841 discriminant analysis (OPLS-DA) was carried out using the ropls (v.1.26.0) package, and
842 metabolites with a VIP > 1, $p < 0.05$, and $|\log FC| > 1$ were identified as differentially abundant
843 metabolites. The abundances of the differentially abundant metabolites in each group were
844 visualized using the ComplexHeatmap (v.2.10.0) package. Spearman correlation analysis was
845 performed on the the metabolome and microbiome data, and the results were visualized using the
846 WGCNA (v.1.70-3) and pheatmap (v.1.0.12) packages, respectively. The Mantel test was
847 performed between the metabolome and microbiome data using the ggcor (v.0.9.4.3) package.
848
849 ***Transcriptome analysis***
850

851 *RNA-seq library construction and sequencing*

852 Total RNA from the colonic epithelial tissue of UC mice was extracted using TRIzol reagent
853 (Invitrogen, America). The RNA-seq libraries were constructed using a TruSeq RNA Sample
854 Prep Kit (Illumina, America) according to the manufacturer's instructions. The polyA+ RNA was
855 enriched, fragmented, and reverse transcribed to obtain cDNA, and end repair, PCR
856 amplification, purification, and quantification were then performed. The libraries were
857 subsequently sequenced on the Illumina NovaSeq 6000 platform.

858

859 *RNA-seq data analysis*

860 The raw data were quality filtered using fastx_toolkit (v.0.0.14), mapped to the mouse genome
861 GRCm39 using Bowtie2 (v.2.4.1), assembled with cufflinks (v.2.2.1), and quantified with RSEM
862 (v.1.1.3).

863 The transcripts per million (TPM) values were used in the following analysis. Low-abundance
864 data were filtered based on the mean TPM values. The differentially expressed genes were
865 defined as those whose p value was <0.05 with the DESeq2 (v.1.34.0) package, and GO and
866 KEGG enrichment analyses were then performed with the clusterProfiler (v.4.2.1) package. The
867 results were visualized using the ggplot2 (v.3.3.5) and ComplexHeatmap (v.2.10.0) packages.

868

869 ***Cell culture***

870 All the cells were maintained at 37 °C in 5% CO_2 in a Heracell 150i incubator (Thermo Fisher

871 Scientific, America). Human NCM460 cells (ATCC) were cultured in RPMI 1640 medium
872 (Gibco, America) supplemented with 10% fetal bovine serum (Gemini, America). Mouse
873 RAW264.7 cells (ATCC) were cultured in DMEM (Gibco, America) supplemented with 10%
874 fetal bovine serum.
875 To assess the anti-inflammatory effects of the HP derivates, RAW264.7 cells were seeded in 96-
876 well plates, stimulated with 100 ng/ml lipopolysaccharide (Sigma–Aldrich, America) for 15 min,
877 and treated with the HP derivates at a concentration of 1 mg/ml for 24 hr. The supernatants were
878 collected and subjected to ELISA.
879
880 ***UC organoid culture***
881 Human UC patient-derived colonoids were cultured as previously described[40,41] with slight
882 modifications. Colon tissue samples were obtained from biopsies taken from male and female
883 UC patients aged 20 to 80 years (inclusive); in all patients, UC had been clearly diagnosed for
884 more than 3 months through clinical manifestations and endoscopic examination. All samples
885 were graded as mild to moderate active ulcerative colitis (Mayo score: 3–10) and were collected
886 at Tsinghua Changgung Hospital (22111–4-02) in Beijing, washed in ice-cold PBS, incubated
887 with 10 mM DTT for 15 min, and disassociated in PBS containing 20 mM EDTA for 60 min at
888 4 °C. The crypts were isolated by vortexing, collected by centrifugation, embedded in growth
889 factor-reduced Matrigel (Corning), and cultured in complete medium consisting of advanced
890 DMEM/F12 (Thermo Fisher Scientific, America) supplemented with 1% penicillin and

891 streptomycin (Thermo Fisher Scientific, America), 10 mM HEPES (Thermo Fisher Scientific,
892 America), 2 mM GlutaMAX (Thermo Fisher Scientific, America), 1 × B-27 supplement (Thermo
893 Fisher Scientific, America), 1 mM N-acetylcysteine (Sigma–Aldrich, America), 100 ng/ml
894 recombinant mouse EGF (Thermo Fisher Scientific, America), 100 ng/ml recombinant human
895 Noggin (PeproTech, America), 1 μg/ml recombinant human R-spondin-1 (PeproTech, America),
896 500 nM A83-01 (Tocris, England), 10 μM SB202190 (Sigma–Aldrich, America) and 10%
897 Afamin/WNT3A conditioned medium (JSR Life Sciences, Japan). To prevent anoikis, 10 mM Y-
898 27632 (STEMCELL Technologies, Canada) was added to the complete medium for the first day
899 of culture. The colonoids were passaged every 6 to 7 days by mechanical disassociation, and the
900 medium was changed every day to ensure their rapid growth.
901
902 ***EdU labeling***
903 EdU labeling of proliferating cells in the colonic epithelia of UC mice was performed on 3-μm
904 sections of paraffin-embedded tissues with a Click-iT EdU Imaging Kit (Invitrogen, America)
905 according to the manufacturer's protocol.
906
907 ***Immunohistochemical and immunofluorescence staining***
908 Paraffin-embedded sections (3 μm thick) were deparaffinized, washed with PBS containing
909 0.01% Tween 20, and subjected to antigen retrieval by immersion in Tris-EDTA buffer (pH 9.0)
910 at 100 °C for 20 min.

911 For immunohistochemical staining, the samples were blocked using peroxidase-blocking
912 solution (Dako, Denmark) and incubated with specific primary antibodies at 4 °C overnight. The
913 fluorescence signals were detected using a REAL EnVision Detection System (Dako, Denmark)
914 and observed using AxioScan. Z1 Slide Scanner (Zeiss, Germay).
915 For immunofluorescence staining, the samples were blocked with 1% BSA/PBS for 1 hr,
916 incubated with specific primary antibodies at 4 °C overnight, and then incubated with secondary
917 antibodies; nuclei were then stained, and the samples were mounted with ProLong Gold Antifade
918 Mountant (Thermo Fisher Scientific, America) and observed using inverted confocal microscopy
919 (Nikon, Japan).
920
921 ***Single-cell RNA sequencing***[42]
922
923 *Preparation of single-cell suspensions from UC organoids*
924 The UC organoids grown on filter paper were placed on an ice-cold plate and allowed to cool for
925 2–3 minutes. The sample wells containing the tissue spheroids to be analyzed were confirmed,
926 the culture medium in the wells was discarded, and the solid Matrigel™ was left. One milliliter
927 of precooled (4 °C) advanced DMEM/F12 culture medium supplemented with 1% HEPES, 1%
928 P/S and 1% GlutaMAX was added to each well, the Matrigel™ surrounding the UC organoids
929 was gently disrupted by pipetting to break it down and dissolve it, and the organoids were
930 collected in 15 mL centrifuge tubes. This procedure was repeated 3 times until all the tissue

931 spheroids were disrupted by pipetting and collected. The mixture was centrifuged at 300 × g and
932 4 °C for 5 minutes, the supernatant was removed, 3 mL of precooled (4 °C) advanced
933 DMEM/F12 culture medium was added to resuspend the pellet, and the mixture was centrifuged
934 again at 200 × g and 4 °C for 5 minutes to remove the supernatant to obtain the colon tissue
935 spheroids. Two milliliters of 0.25% trypsin was added to the suspension, which was subsequently
936 incubated at 37 °C in a water bath for 5 minutes, after which an equal volume of RPMI-1640
937 medium containing 10% fetal bovine serum (FBS) was added to terminate the enzymatic
938 digestion. A 1 mL pipet was used to pipet the suspension ten times. The suspension was
939 centrifuged at 300 × g and 4 °C for 5 minutes, and the supernatant was removed. Then, 2 mL of
940 0.0005% Y-27632/TrypLE was added to generate a suspension, which was incubated at 37 °C in
941 a water bath for 15 minutes and pipetted ten times at 5-minute intervals. After the incubation was
942 complete, an equal volume of RPMI-1640 medium containing 10% FBS was added to terminate
943 the reaction. The suspension was centrifuged at 400 × g and 4 °C for 5 minutes, and the
944 supernatant was removed. Then, 50–200 μL of RPMI-1640 medium containing 10% FBS was
945 added to generate a suspension so that the cell concentration was within the range of 700–1200
946 cells/μL. This suspension was disrupted by vigorous pipetting ten to twenty times to obtain
947 single cells from the UC organoids.
948
949 *Single-cell RNA sequencing and library construction for colonic organoids*
950 The concentration and viability of the cells in the single-cell suspensions of colonic organoids

951 were measured with a cell counter. Samples with a cell viability greater than 80%, an
952 agglomeration rate of less than 5% and a lack of obvious cell debris or impurities were
953 considered suitable for library construction. Using microfluidic technology, gel beads and
954 individual cells with specific cell barcodes and reverse transcription information were coated
955 with oil droplets. The cells were solubilized and released mRNA in this system, and the mRNA
956 was captured by the gel beads and reverse transcribed to generate the full-length cDNA
957 sequence. The oil droplets were then disrupted and purified, the amount of cDNA was increased
958 by PCR amplification, and the sequencing primers were ligated. The cDNA was cleaved into
959 fragments of approximately 200~300 bp by a chemical method, end repair was carried out, P7
960 adapters were connected, sample barcodes were introduced, and the sequence fragments were
961 screened. The library was sequenced on the Illumina NovaSeq platform with a PE150
962 sequencing strategy.
963 The unique molecular identifiers (UMIs) in the off-machine data were preprocessed using
964 CellRanger software, an official tool of 10x Genomics. Loupe Browser 6 software, an official
965 tool of 10x Genomics, was used to delete the multicell data, low-quality data, and apoptotic cell
966 data. The corresponding data barcode criteria were a UMI count of greater than 60,000, a feature
967 count of less than 210, and a percentage of mitochondrial UMIs of greater than 25%. Afterward,
968 the uniform manifold approximation and projection (UMAP) method was used for
969 dimensionality reduction. After dimensionality reduction, the CellRanger off-machine data were
970 imported into R Studio, and Seurat was used for dimensionality reduction classification.

Data availability

All the data supporting the results of this study are available within the paper and its Supplementary Materials. Additional processed data are available from the corresponding authors upon request.

Methods references

40. Fujii, M., Matano, M., Nanki, K. & Sato, T. Efficient genetic engineering of human intestinal organoids using electroporation. *Nat. Protoc.* **10**, 1474–1485 (2015).

41. Sato, T. et al. Long-term expansion of epithelial organoids from human colon, adenoma, adenocarcinoma, and Barrett's epithelium. *Gastroenterology* **141**, 1762–1772 (2011).

42. Hao, Y. et al. Dictionary learning for integrative, multimodal and scalable single-cell analysis. *Nat. Biotechnol.* **42**, 293–304 (2024).

Acknowledgments

We thank the National Center for Electron Microscopy in Beijing, School of Materials Science, Tsinghua University, for assistance with electron microscopy imaging; the Laboratory Animal Resources Center, Tsinghua University, for technical support; and the Center of Biomedical Analysis, Tsinghua University, for assistance with imaging technology and flow cytometry; Key Research and Development Program of the Ministry of Science and Technology (2023YFA0914300) and Shenzhen Medical Research Fund (SMRF, B2302009), for regarding financial assistance.

Author contributions

XH. X., Y. W. and X. J. oversaw the research. W. H., L. H., Y. W., W. Z. and XH. X. designed the research strategy. W. H., XY. R and W. Z. established the ulcerative colitis organoids. W. H., L. H., ZK. L., QX. Z., W. Z, and XY. R. performed the experiments. W. H., Y. W., and ZQ. Z. analyzed the experimental data. W. H., Y. W., and XH. X. prepared the manuscript. YS. Y., HC. Z and Y. C. provided the materials for the experiments and critical review of manuscript. All the authors approved the manuscript.

Competing interests

XH. X., W. H. and Y. W. are inventors on related patents filed by Tsinghua University describing the materials reported in this study. The other authors declare that they have no competing

interests.

1008 **Extended Data**

1009 **Extended Data Fig.1| Therapeutic efficacy evaluation of the library of non-anticoagulated**

1010 **heparin derivates.**

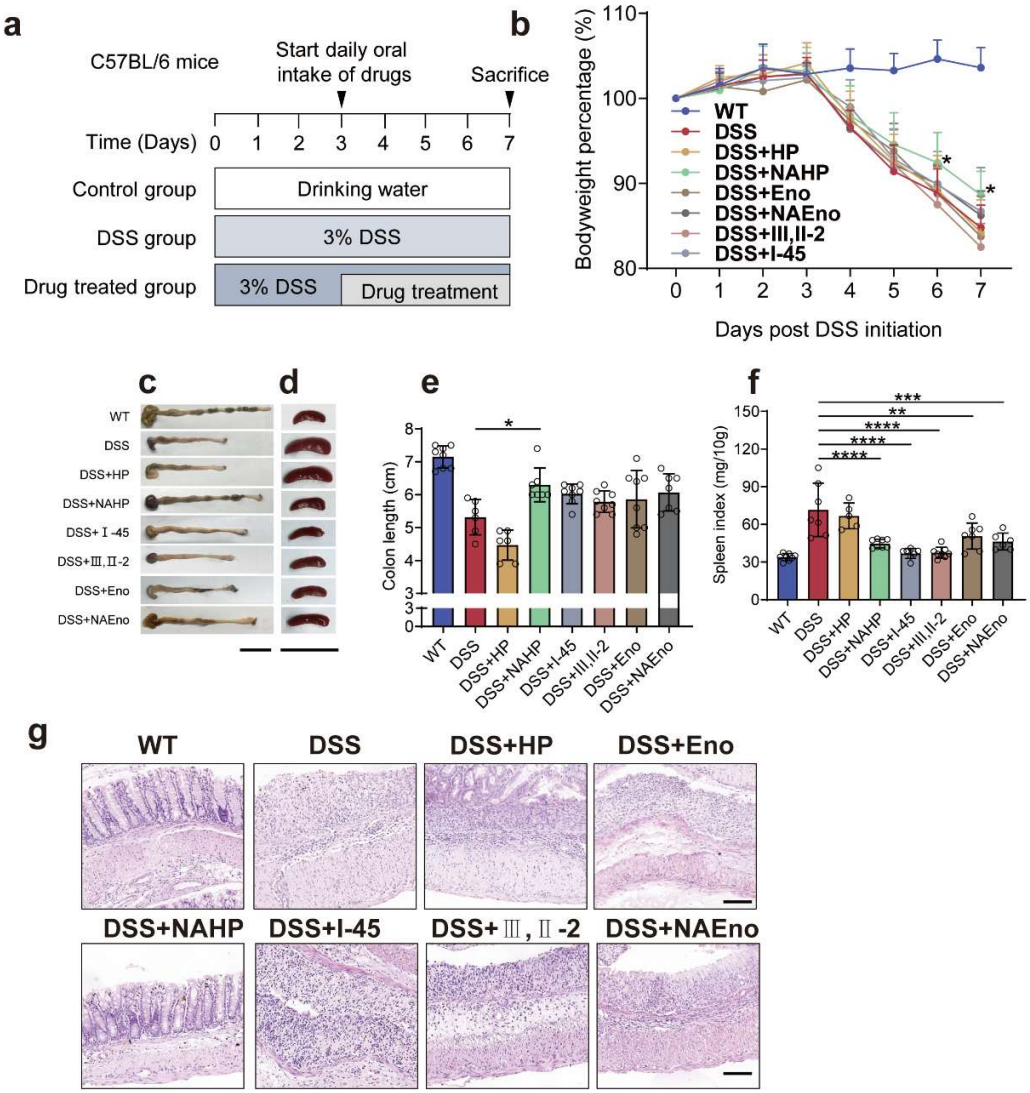

1011

1012 **a,** 3%DSS was added to the drinking water for 7 days to induce acute colitis in mice (n=10). The

1013 control group of mice was given regular drinking water (n=10), and the drug treatment group was

1014 given 30mg/kg heparin (HP), Enoxaparin (Eno), Non-anticoagulated heparin (NAHP), Non-

1015 anticoagulated Enoxaparin (NAEno), Heparin digested by heparinase I(I-45), Heparin digested by
1016 heparinase II and heparinase III(III-II-2) on the third day (n=10). **b,** Changes in weight **c-f,** Mice
1017 were scarified on day 7 and colon (**c**) and spleen (**d**) were collected, Colon length (**e**) and Spleen
1018 index (**f**) were quantitated. **g,** Representative images of colons stained with Hematoxylin and eosin,
1019 Scale bar, 100μm. Shown (**b, e, f**) are representative images or quantitative analysis from at least
1020 n=5 biologically independent samples. Data represent mean ±SD. * $p < 0.05$, ** $p < 0.01$, *** $p <$
1021 0.001, **** $p < 0.0001$ and ns (no significance) $p > 0.05$, analyzed by ordinary one-way ANOVA
1022 (**b**) multiple comparisons test.
1023

Extended Data Fig.2| Therapeutic efficacy evaluation of different molecular weight NAHP.

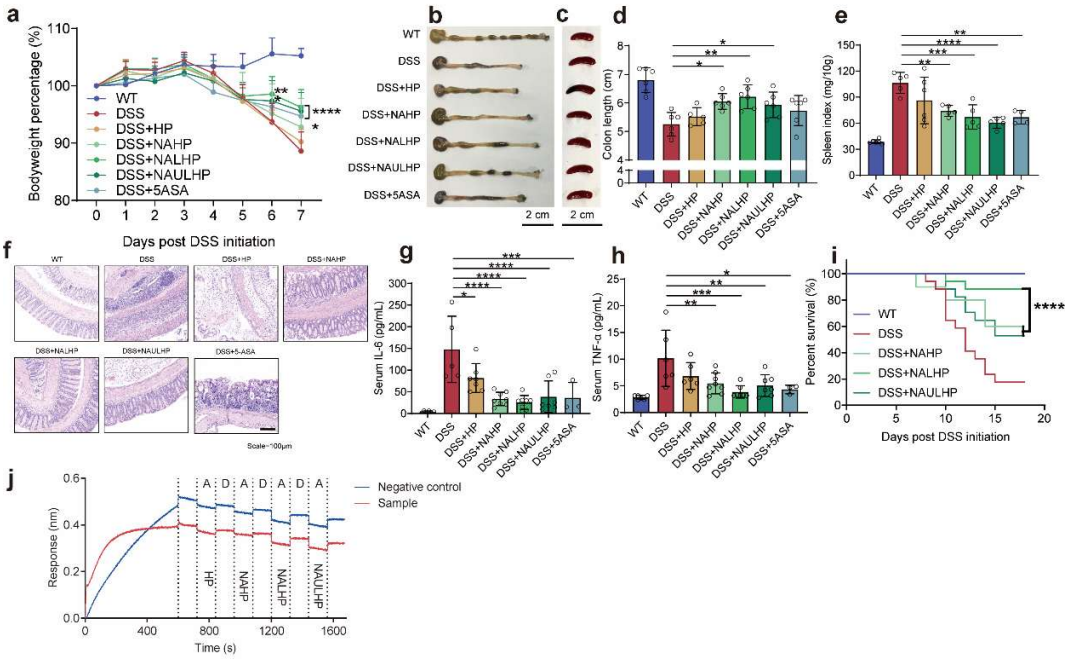

a, Changes in weight **b-e,** Mice were scarified on day 7 and colon (**b**) and spleen (**c**) were collected, Colon length (**d**) and Spleen index (**e**) were quantitated. **f,** Representative images of colons stained with Hematoxylin and eosin, Scale bar, 100μm. **g,h,** The concentration of Serum IL-6 (**g**) and TNF-α (**h**) were determined by ELISA when mice were scarified on day 7. **i,** The death status of mice after being modeled with DSS and treated with NAHP, NALHP and NAULHP. **j,** The adsorption(A) and desorption(D) response curves among HP, NAHP, NALHP, NAULHP and DSS by Bio-Layer Interferometry (BLI), blue line represents the blank contrast, orange line represents the sample.

Shown (**a, d, e, g-l**) are representative images or quantitative analysis from at least n=5 biologically independent samples. Data represent mean ±SD. * $p < 0.05$, ** $p < 0.01$, *** $p < 0.001$, **** $p <$

1036 0.0001 and ns (no significance) $p > 0.05$, analyzed by ordinary one-way ANOVA (**a**) multiple

1037 comparisons test.

1038

Extended Data Fig. 3| The physicochemical properties of heparin derivates.

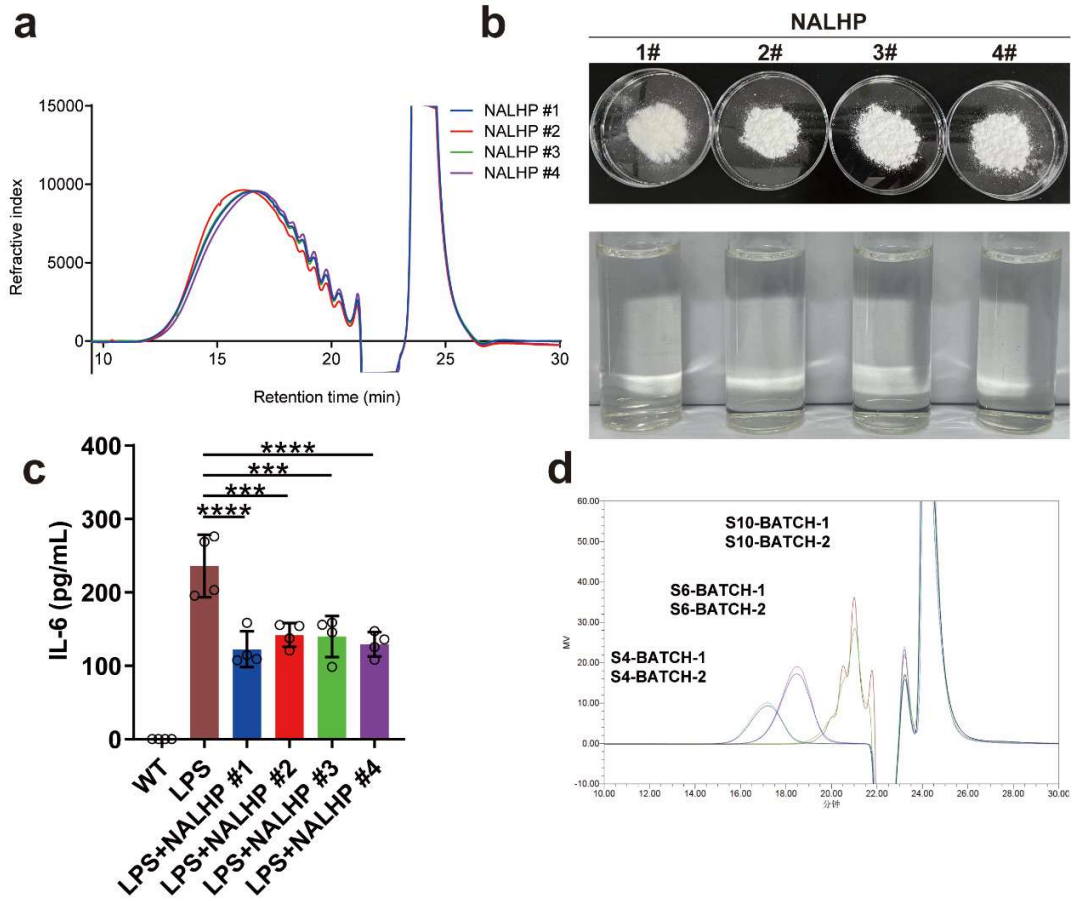

a, Gel chromatograms of four batches production of NALHP. **b,** The morphology and solubility of NALHP prepared by four batches (#1-#4). **c,** The concentration of IL-6 factor in the cell supernatant of RAW264.7 cells after treatment with the four batches of NALHP. **d**, Gel exclusion chromatograms of the separated components from two batches (BATCH-1 and -2). Shown (**c**) are representative images or quantitative analysis from n=4 biologically independent samples. Data represent mean ±SD. * $p < 0.05$, ** $p < 0.01$, *** $p < 0.001$, **** $p < 0.0001$ and ns (no significance) $p > 0.05$, analyzed by ordinary one-way ANOVA (**g**) multiple comparisons test.

Extended Data Fig.4 | Therapeutic efficacy evaluation of different non-anticoagulated heparin derivates.

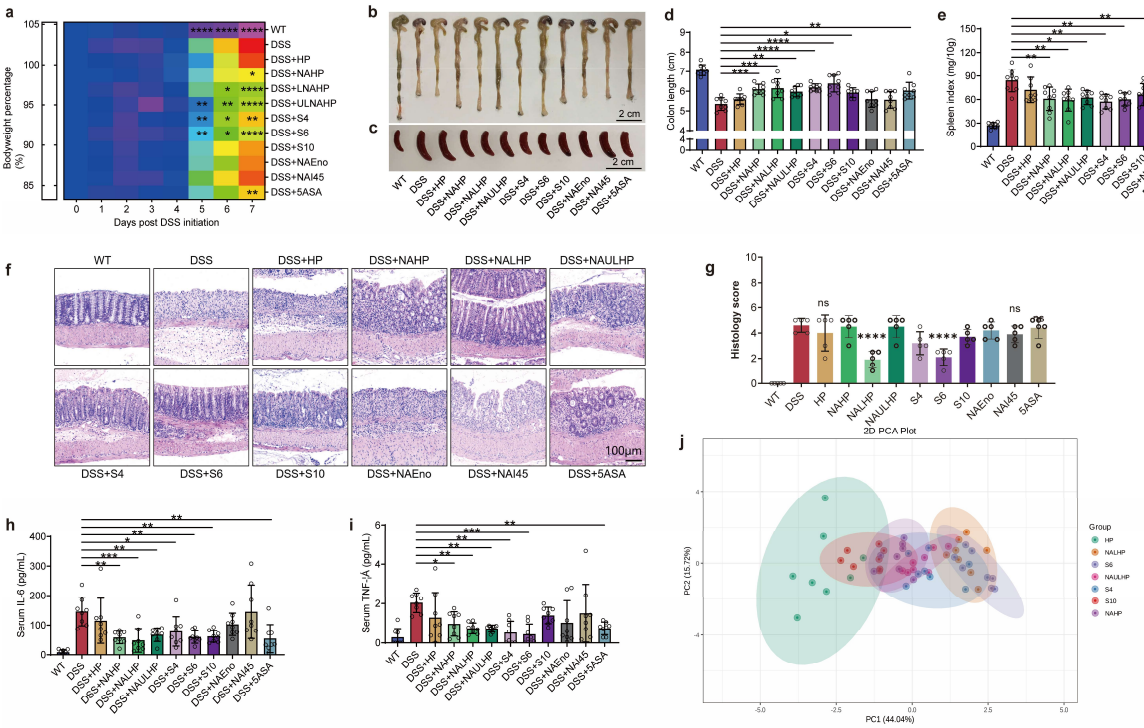

a, Changes in weight. **b-e,** Mice were scarified on day 7 and colon (**b**) and spleen (**c**) were collected, Colon length (**d**) and Spleen index (**e**) were quantitated. **f,** Representative images of colons stained with Hematoxylin and eosin, and Histological score (**g**) were quantified. Scale, 100μm. **h,i,** The concentration of Serum IL-6 (**h**) and TNF-α (**i**) were determined by ELISA when mice were scarified on day 7. j, Principal component analysis of phenotypes pertaining to UC treatment by HP, NAHP, NALHP, NAULHP, S4, S6 and S10.

Shown (**d, e, g-i**) are representative images or quantitative analysis from n=6 biologically independent samples. Data represent mean ±SD. * $p < 0.05$, ** $p < 0.01$, *** $p < 0.001$, **** $p < 0.0001$ and ns (no significance) $p > 0.05$, analyzed by ordinary one-way ANOVA (**a**) multiple

1061 comparisons test. The data obtained from the PCA analysis represent the improvement in the
1062 characteristics of UC mice (including body weight, colon length, spleen index, serum IL-6 and
1063 TNF-α levels, and histological scores) treated with drugs of different molecular weights (HP,
1064 NAHP, NALHP, NAULHP, S4, S6 and S10).
1065
1066

1067 **Extended Data Table.1** The molecular weight size and distribution of NALHP and its fine
1068 fragments

Name	Separation(mg)	Content (%, w/w)	M_w （Da）	P	M_w（Da）Distribution（%）			
					>8k	5k~8k	3k~5k	<3k
NALHP	650	100	6224	2.33	28.04	27.87	19.11	24.95
NAULHP	-	-	2974	3.22	5.21	14.96	20.05	59.77
S1	37.7	5.8	12121	1.036	99	1		
S2	44.2	6.8	9557	1.037	80	20		
S3	42.9	6.6	7686	1.038	38	60	2	
S4	37.7	5.8	6254	1.041	8	78	13	
S5	89.7	13.8	5094	1.055	1	50	46	2
S6	99.5	15.3	4115	1.076		19	68	13
S7	71.5	11.0	3227	1.117		5	50	45
S8	78.65	12.1	2426	1.172		1	23	76
S9	62.4	9.6	1736	1.188			7	93
S10	48.1	7.4	1282	1.153			1	99
S11	37.7	5.8	812	1.073				100

1069

1070

1071

1072

1073

Extended Data Fig.5| Heteronuclear singular quantum correlation (HSQC) of different heparin derivates.

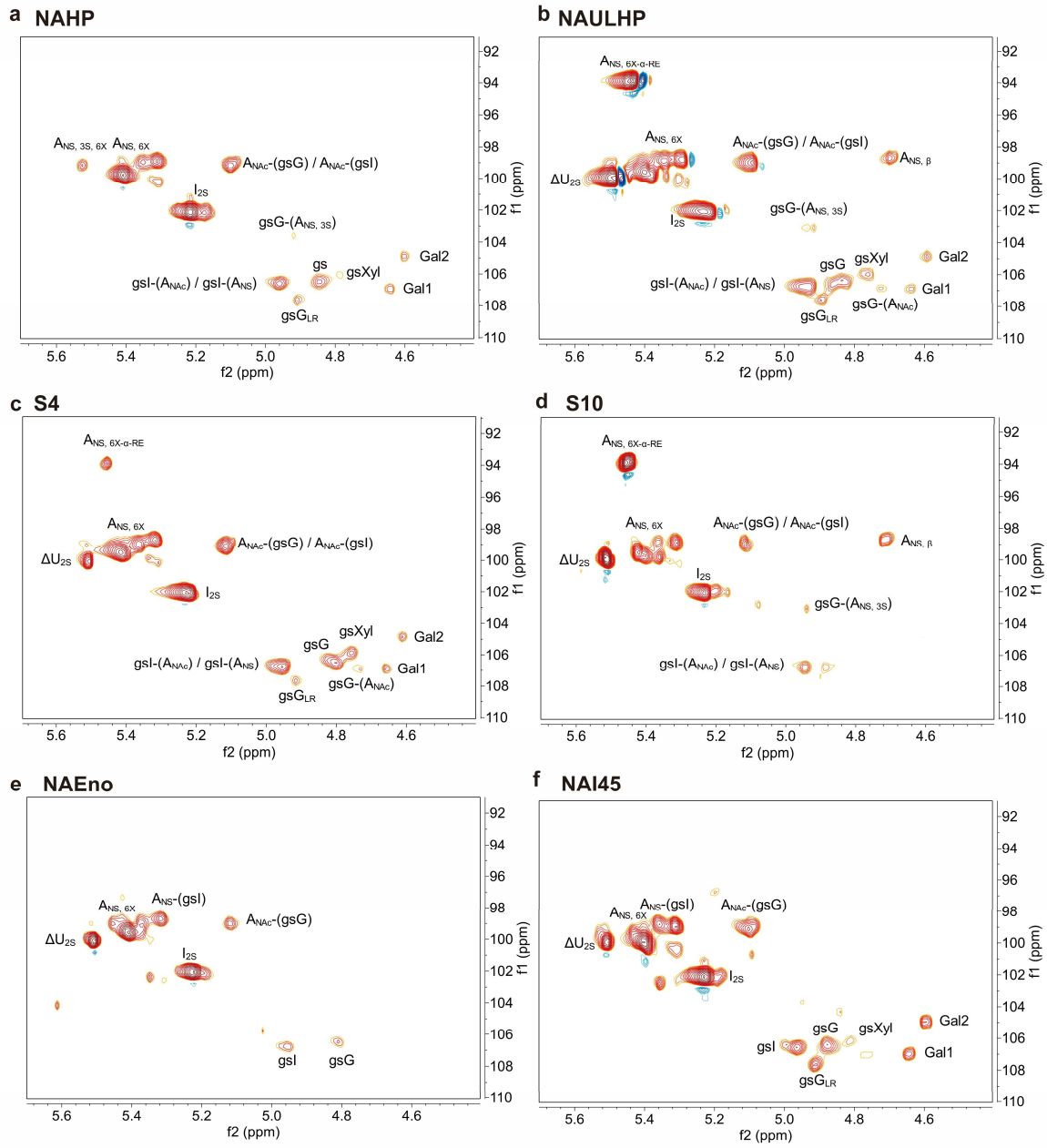

a, HP. **b,** NAHP. **c,** S4. **d,** NAULHP**. e,** S10. **f,** NAI45.

1081 **Extended Data Fig. 6| Infrared spectra of different heparin derivates.**

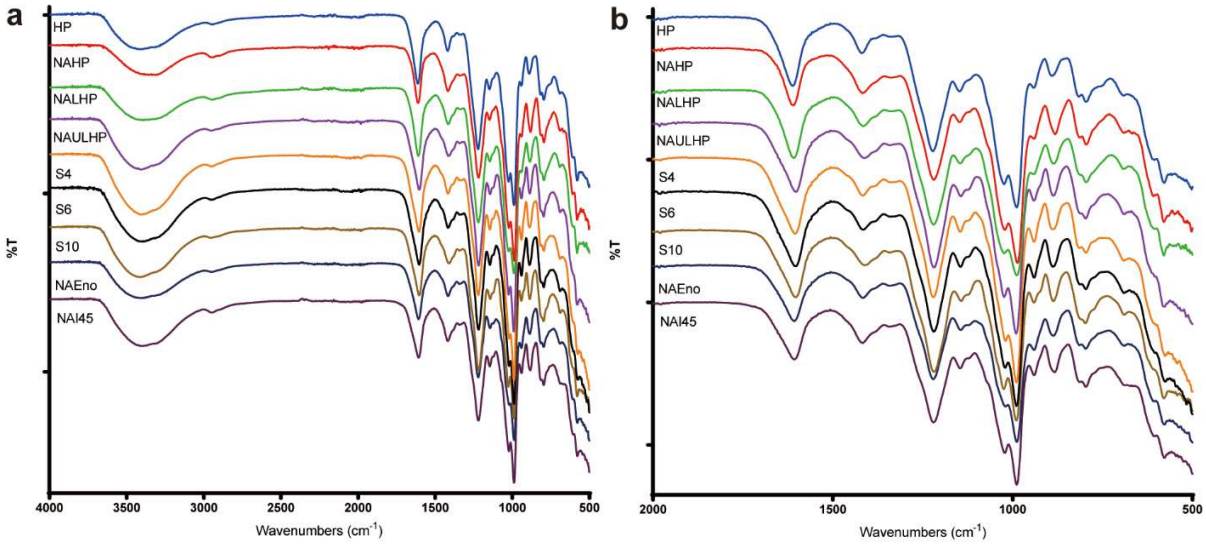

1082

1083 **a,** Infrared full spectrum of heparin derivates. **b,** Infrared spectra between 2000 cm^{-1} and 500 cm^{-}

1084 ^{1} of heparin derivates.

1085

1086

1087

1088 **Extended Data Table.2** Infrared spectral characteristic peak information of heparin-like
1089 polysaccharides

Wave (cm^{-1})	Source of characteristic peaks	Type of characteristic peak
800	IdoA**2S**	C-O-S stretching and vibration peak
820	GlcNS**6S**	C-O-S stretching and vibration peak
890	Glc**NS**	C-O-S stretching and vibration peak、 C-O-C Vibration coupling peak
940	GlcNS**6S**	C-O-S stretching and vibration peak、 C-O-C glycosidic bond
1230	Glc**NS**	S=O Asymmetric stretching vibration peak
1378	GlcN**Ac**	$-CH_3$ Vibration peak
1560	GlcN**Ac**	Amide bond

1090

1091

1092

Extended Data Table.3 The batch numbers of raw materials and products of 4 batches of NALHP production

Batch Number	#1	#2	#3	#4
HP	NHS210204	NHS200606	NHS200803	NHS180302
NAHP	BATCH-211019	BATCH-210401	BATCH-210319	BATCH-190304
NALHP	BATCH-211023	BATCH-210408	BATCH-210402	BATCH-190504

Extended Data Table.4 Preparation process parameter standards for 4 batches of NALHP production

Process Indicators	#1	#2	#3	#4	Process standard	Qualified or unqualified
anti-Xa（IU/mg）	19.4	18.1	18.5	19.0	<20	Qualified
A_{232}	19.0	12.2	28.1	23.4	<30	Qualified
ΔA_{232}	41.0	39.7	38.8	39.6	39.5±2.0	Qualified
A_{294}	0.167	0.134	0.189	0.245	<0.350	Qualified
A_{420}	0.018	0.019	0.015	0.022	<0.025	Qualified
NALHP ΔM_w（Da）	102	136	150	242	-300~300	Qualified

Extended Data Table.5 The molecular weight size and distribution of 4 batches of NALHP production

Batch number	M_w（Da）	ΔM_w（Da）	P	M_w（Da）Distribution（%）			
				>8k	5k~8k	3k~5k	<3k
#1	6326	102	1.505	28	34	20	18
#2	6360	136	1.494	29	33	21	17
#3	6374	150	1.573	30	32	19	19
#4	6466	242	1.548	31	29	21	19
Standard	6224	0	1.531	28	32	21	19

1107 **Extended Data Fig.7 | ^{13}C NMR spectrum of different heparin derivates.**

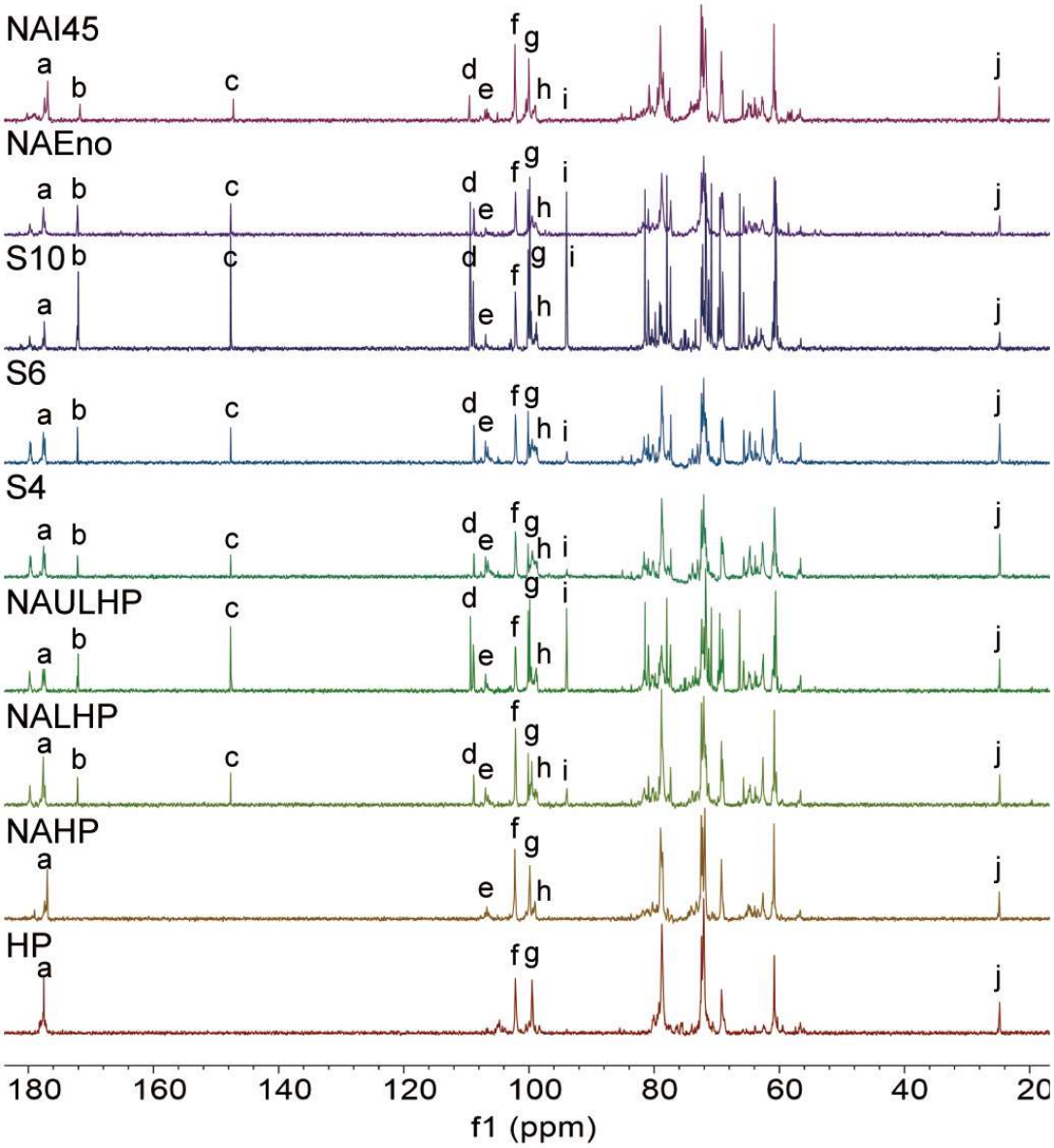

1108

1109

1110 **Extended Data Table.6** ^{13}C NMR chemical shift attribution of HP and different non-
1111 anticoagulated heparin derivates

Peak position	Test the chemical shift of the sample（ppm）							Chemical shift attribution
	HP	NAHP	NALHP	NAULHP	S4	S6	S10	
a	177.7	176.7	177.7	177.7	177.7	177.7	177.7	U, -**C**OOH; GlcNAc6S / GlcNAc, CH_3**C**O-
b	-	-	172.1	172.1	172.1	172.1	172.1	ΔU / ΔU2S, -**C**OOH
c	-	-	147.6	147.6	147.6	147.6	147.6	ΔU2S, **C5**
d	-	-	108.9	108.9	108.9	108.9	108.9	ΔU2S, **C4**
e	-	106.7	106.7	106.7	106.7	106.7	106.7	gsIdoA / gsGlcA, **C1**
f	102.3	102.3	102.3	102.3	102.3	102.3	102.3	IdoA2S, **C1**
g	99.9	99.9	99.9	99.9	99.9	99.9	99.9	ΔU2S / GlcNS6S / GlcNS / GlcNAc6S / GlcNAc, **C1**
h	-	99.1	99.1	99.1	99.1	99.1	99.1	**GlcNAc**-(gsIdoA)/ **GlcNAc**-(gsGlcA), **C1**
i	-	-	93.9	93.9	93.9	93.9	93.9	GlcNS-α-RE
j	24.8	24.8	24.8	24.8	24.8	24.8	24.8	-**C**H_3CO-

1112

1113

1114

1115

1116

1117

1118 **Extended Data Fig.8| ^{1}H NMR spectrum of different heparin derivates.**

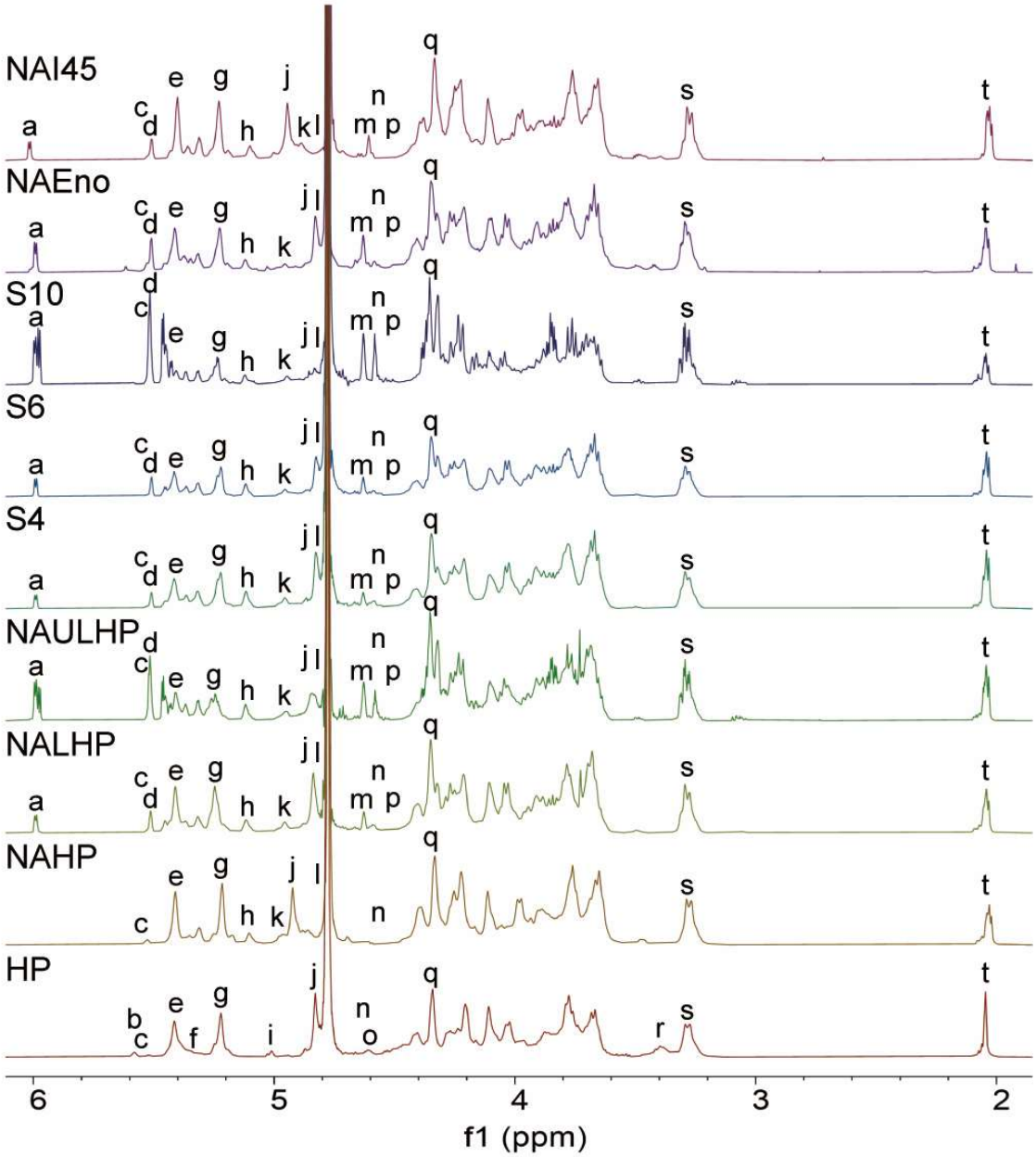

1119

1120

Extended Data Table.7 ^{1}H NMR chemical shift attribution of HP and different non-anticoagulated heparin derivates

Peak position	Test the chemical shift of the sample（ppm）							Chemical shift attribution
	HP	NAHP	NALHP	NAULHP	S4	S6	S10	
a	-	-	5.99	5.99	5.99	5.99	5.99	ΔU, **H4**
b	5.58	-	-	-	-	-	-	**GlcNS**-(GlcA), **H1**
c	5.53	5.53	5.53	5.53	5.53	5.53	5.53	GlcNS3S6S, **H1**
d	-	-	5.52	5.52	5.52	5.52	5.52	ΔU, **H1**
e	5.42	5.42	5.42	5.42	5.42	5.42	5.42	GlcNS6S / GlcNAc6X / **GlcNS6X**-(gsIdoA) / **GlcNS6X**-(gsGlcA), **H1**
f	5.35	-	-	-	-	-	-	**GlcNS6X**-(IdoA), **H1**
g	5.22	5.22	5.22	5.22	5.22	5.22	5.22	IdoA2S, **H1**
h	-	5.12	5.12	5.12	5.12	5.12	5.12	**GlcNAc**-(gsIdoA)/ **GlcNAc**-(gsGlcA), **H1**
i	5.01	-	-	-	-	-	-	**IdoA**-(GlcNS), **H1**
j	4.83	4.92	4.83	4.83	4.83	4.83	4.83	IdoA2S, **H5**
k	-	4.97	4.97	4.97	4.97	4.97	4.97	gsIdoA, **H1**
l	-	4.85	4.85	4.85	4.85	4.85	4.85	gsGlcA, **H1**
m	-	4.73	4.73	4.73	4.73	4.73	4.73	gsXyl, **H1**
n	4.64	4.64	4.64	4.64	4.64	4.64	4.64	Gal, **H1**
o	4.61	-	-	-	-	-	-	GlcA, **H1**
p	-	-	4.63	4.63	4.63	4.63	4.63	ΔU, **H2**
q	4.34	4.34	4.34	4.34	4.34	4.34	4.34	IdoA2S, **H2**
r	3.40	-	-	-	-	-	-	GlcA, **H2**
s	3.28	3.28	3.28	3.28	3.28	3.28	3.28	GlcNS6X, **H2**
t	2.05	2.05	2.05	2.05	2.05	2.05	2.05	-C**H**$_3$CO

Extended Data Fig. 9| Therapeutic efficacy evaluation of the library of S6.

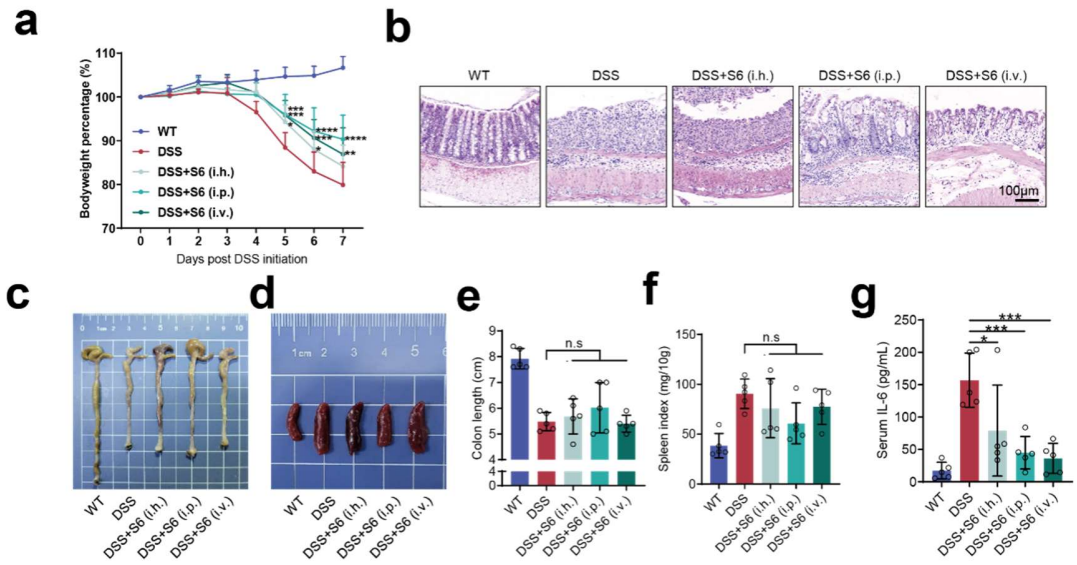

a, The body weight changes of mice under different administration methods (Intravenous injection(i.v.), intraperitoneal injection(i.p.), hypodermic injection(i.h.)). **b,** The body weight changes of mice under different administration methods. **c-f,** Mice were scarified on day 7 and colon (**c**) and spleen (**d**) were collected, Colon length (**e**) and Spleen index (**f**) were quantitated. **g,** The concentration of Serum IL-6 was determined by ELISA when mice were scarified on day 7. Shown (**a, e-g**) are representative images or quantitative analysis from at least n=5 biologically independent samples. Data represent mean ±SD. * $p < 0.05$, ** $p < 0.01$, *** $p < 0.001$, **** $p < 0.0001$ and ns (no significance) $p > 0.05$, analyzed by ordinary one-way ANOVA (**g**) multiple comparisons test.

Extended Data Fig.10| Microbiological and metabolome analysis.

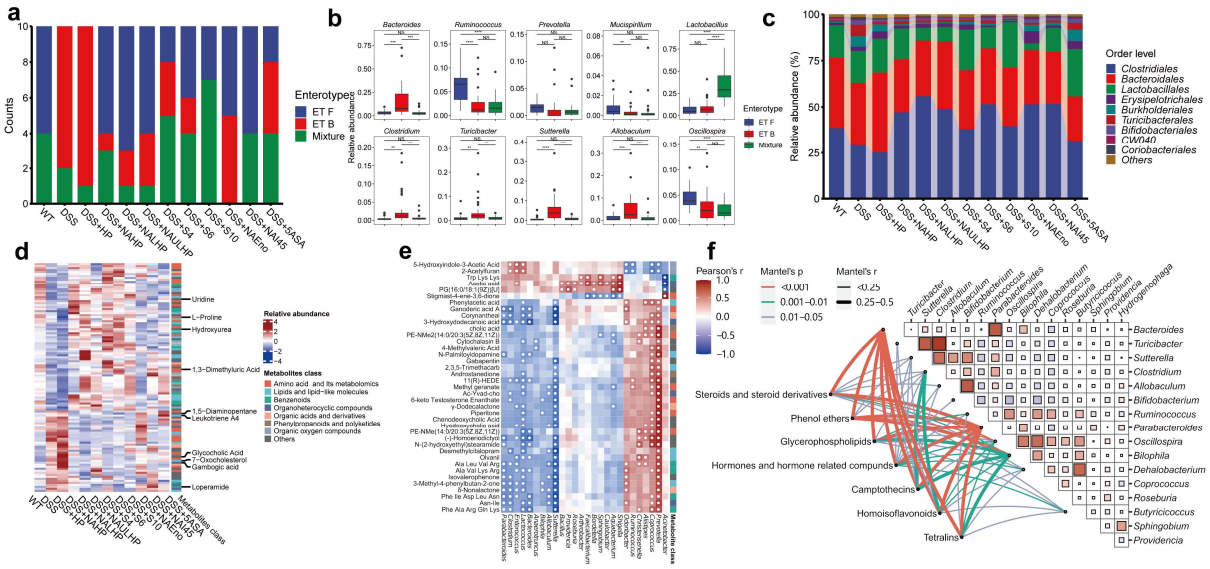

a, Intestinal type analysis under the action of different heparin derivates. **b,** The distribution of marker flora at the genus level in the DMM classification model. **c,** The composition of intestinal flora at the genus level in each experimental group. **d,** Changes in metabolites among different experimental groups**. e,** Spearman correlation analysis of the microbiome and metabolome. **f,** Mantel analysis of the microbiome and metabolome.

1144 **Extended Data Fig.11| Transcriptome analysis of the colons of UC and drug-treated mice.**

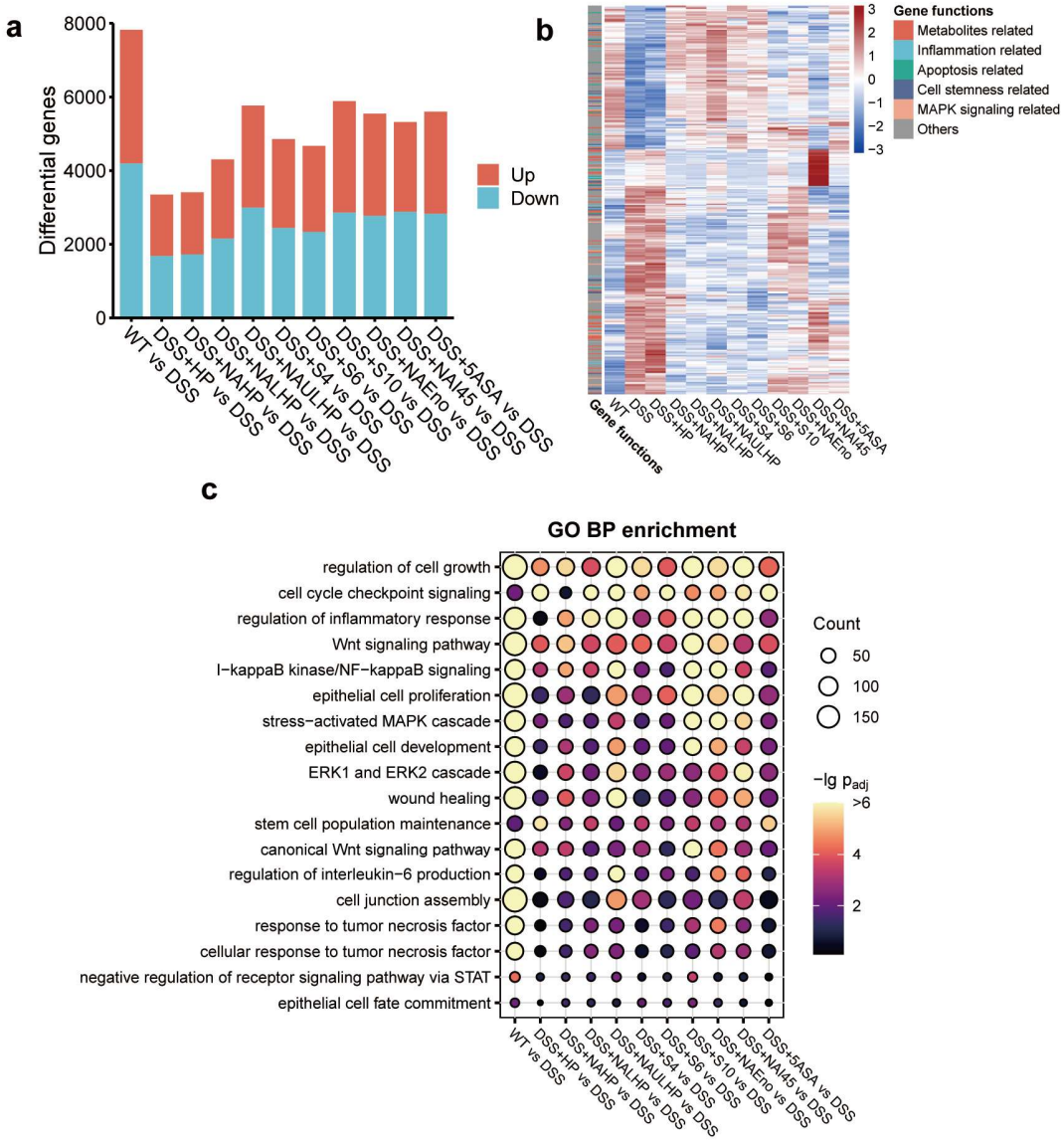

1145

1146 **a,** Differential genes analysis. **b,** Enrichment analysis of differential genes. **c,** GO enrichment

1147 analysis of differential genes under the action of different heparin derivates.

1148

1149 **Extended Data Fig.12| The expression level of TCF1 in the colonic submucosal layer of UC**

1150 **mice.**

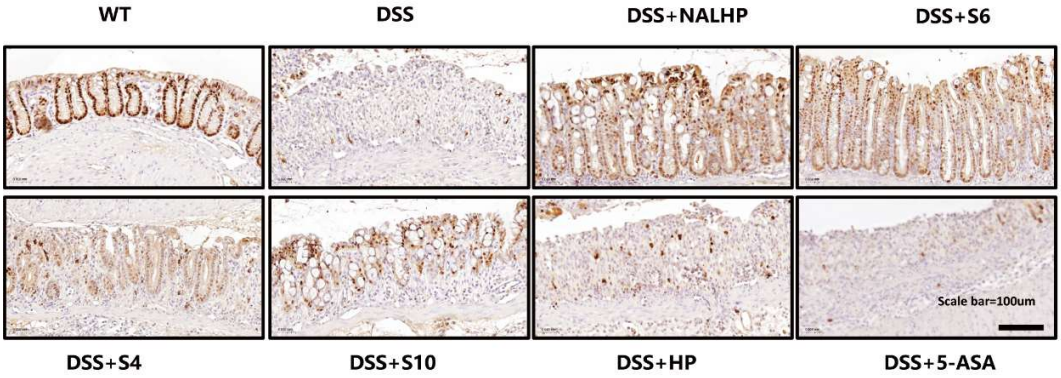

1151

1152 Representative images of immunohistochemical staining for TCF1 in healthy and UC mice

1153 treated by water, NALHP, S6, S4, S10, HP and 5-ASA. Scale bar, 100 μm. Representative

1154 images from n= 5 biologically independent samples are shown.

1155

1156

1157 **Extended Data Fig.13| The expression level of PCNA in the colonic submucosal layer of UC**
1158 **mice.**

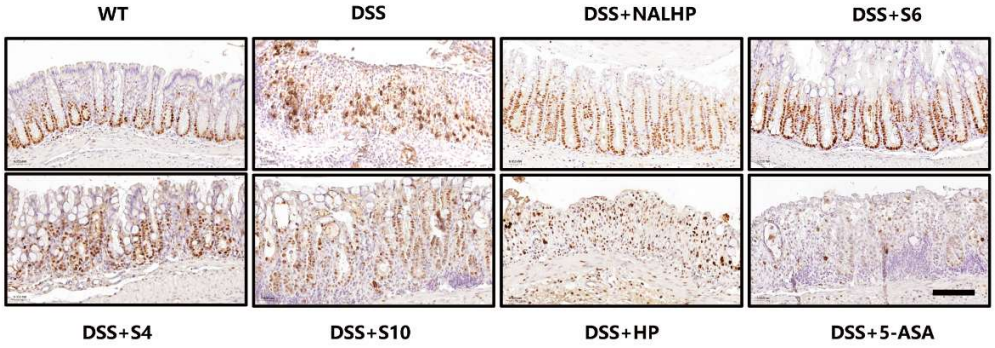

1159

1160 Representative images of immunohistochemical staining for PCNA in healthy and UC mice

1161 treated by water, NALHP, S6, S4, S10, HP and 5-ASA. Scale bar, 100 μm. Representative

1162 images from n= 5 biologically independent samples are shown.

1163

1164

1165

1166

1167

1168

Extended Data Fig.14| The expression levels of MUC2 and PCNA vary among human [1], mice, and organoids.

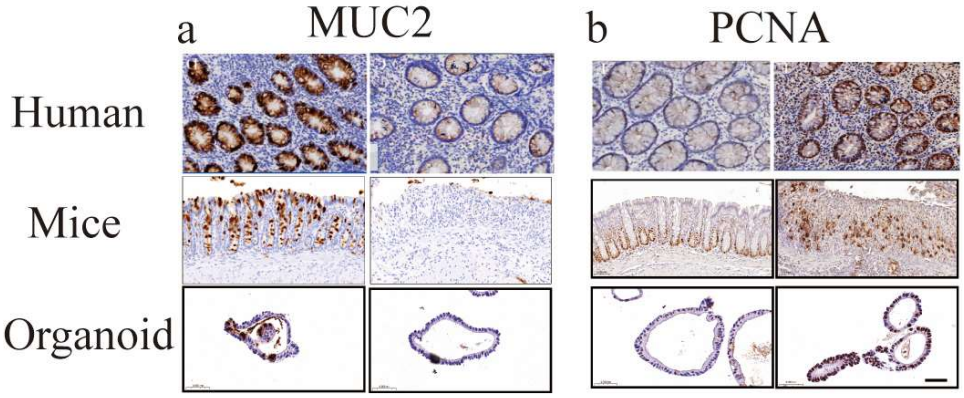

Representative images of immunohistochemical staining for MUC2(a) and PCNA(b) in human, mice and organoids. Scale bar, 50 μm. Representative images from n= 3 biologically independent samples are shown.

[1] He, T., Wang, W., Li, L., Qiu, S., Sun, S., & Zong, L. (2022). PCNA, EGFR, MUC2 expression levels and clinical significance in ulcerative colitis. *Journal of Medical Research*, *51*(3), 104-107.

Extended Data Fig.15| Single-cell transcriptome analysis.

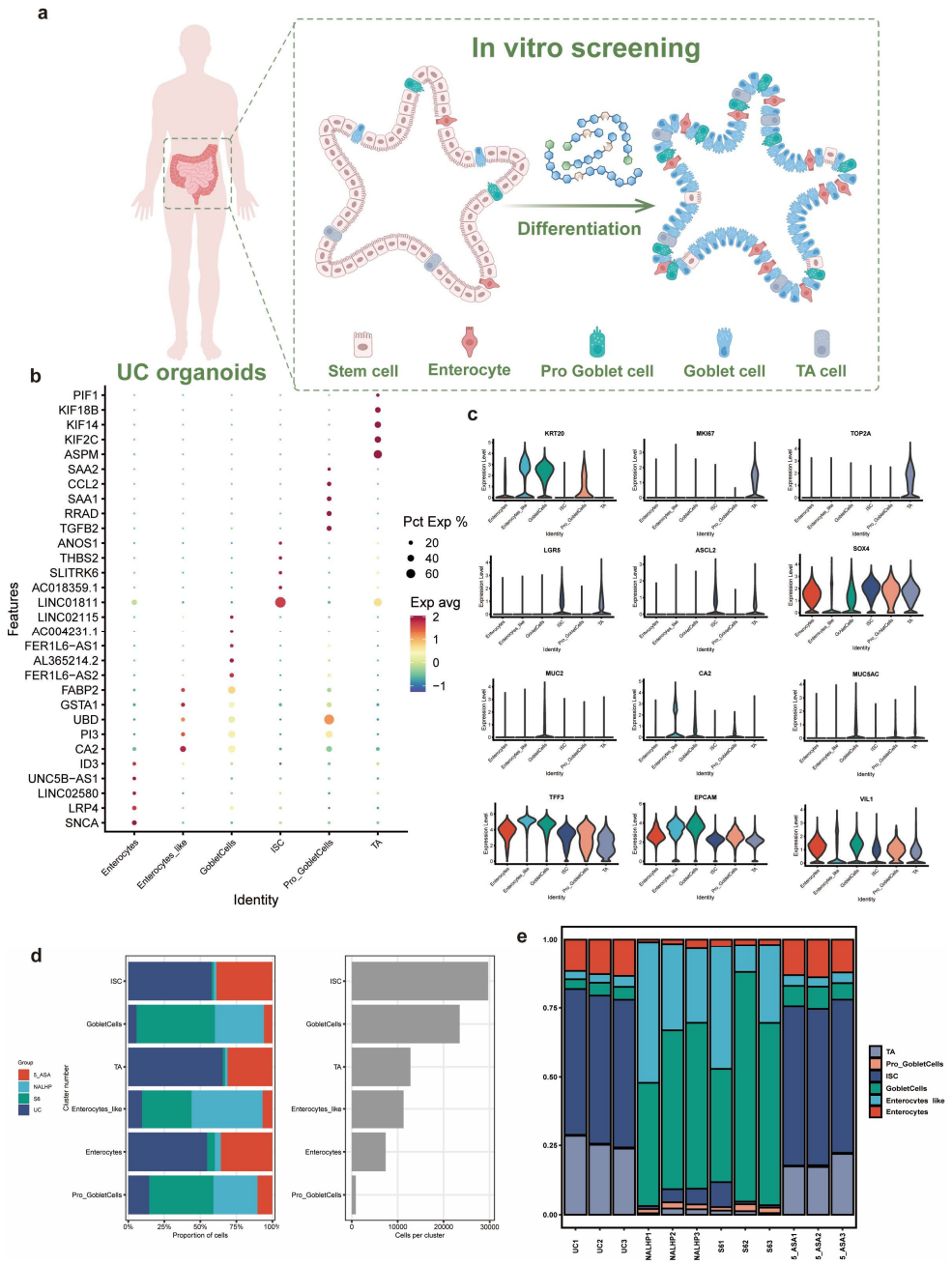

a, The proportion of cells in different groups. **b,** The changes in cell types of organoids under the action of heparin derivates. **c,** Cell typing criteria. **d,** The expression of genes in different cell types. **e,** Schematic diagram of cell type changes in UC organoids.

Extended Data Fig.16 | Pseudotime Analysis reveals the trajectory of stem cells differentiating into goblet cells in organoids

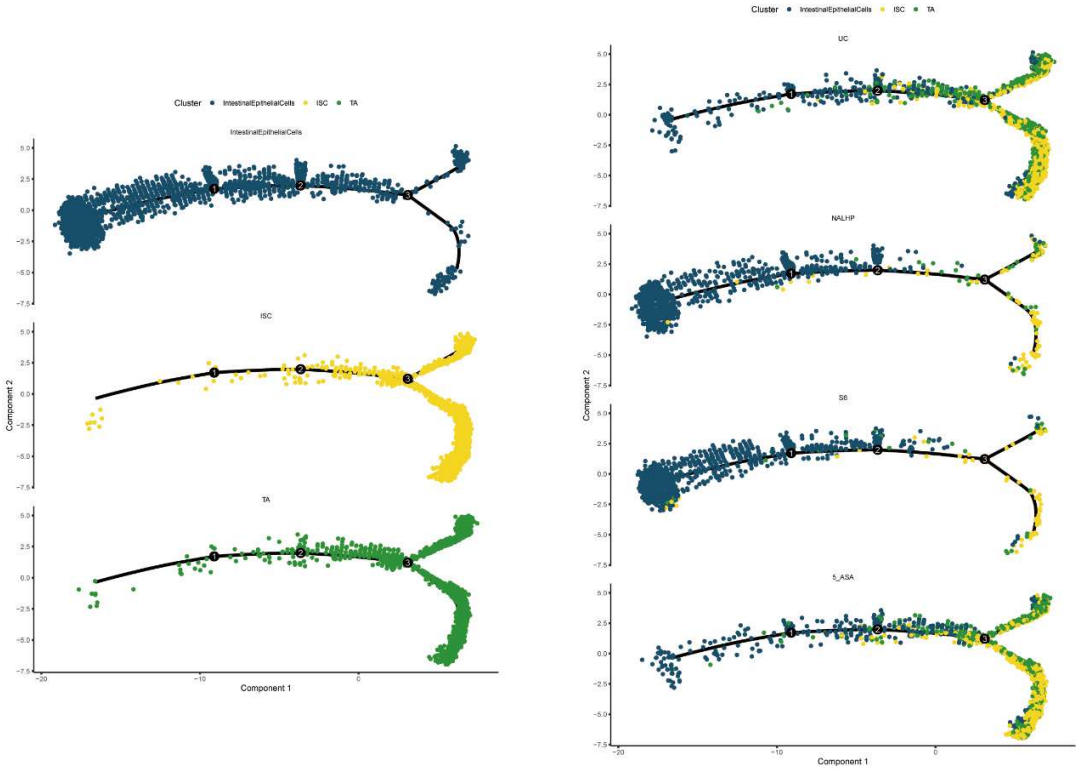

The single-cell RNA-seq data from stem cells of UC-type organs were subjected to time-series analysis (using Monocle2) under different cell types **(a)** and different group **(b)**. The cells were arranged on a continuous trajectory based on their transcriptional status. The cells were sorted according to pseudo-time, and genes were clustered according to their expression patterns (blue: intestinal epithelial cells; yellow: intestinal stem cells; green: TA cells).

Extended Data Fig.17 | U-map dimensionality reduction analysis.

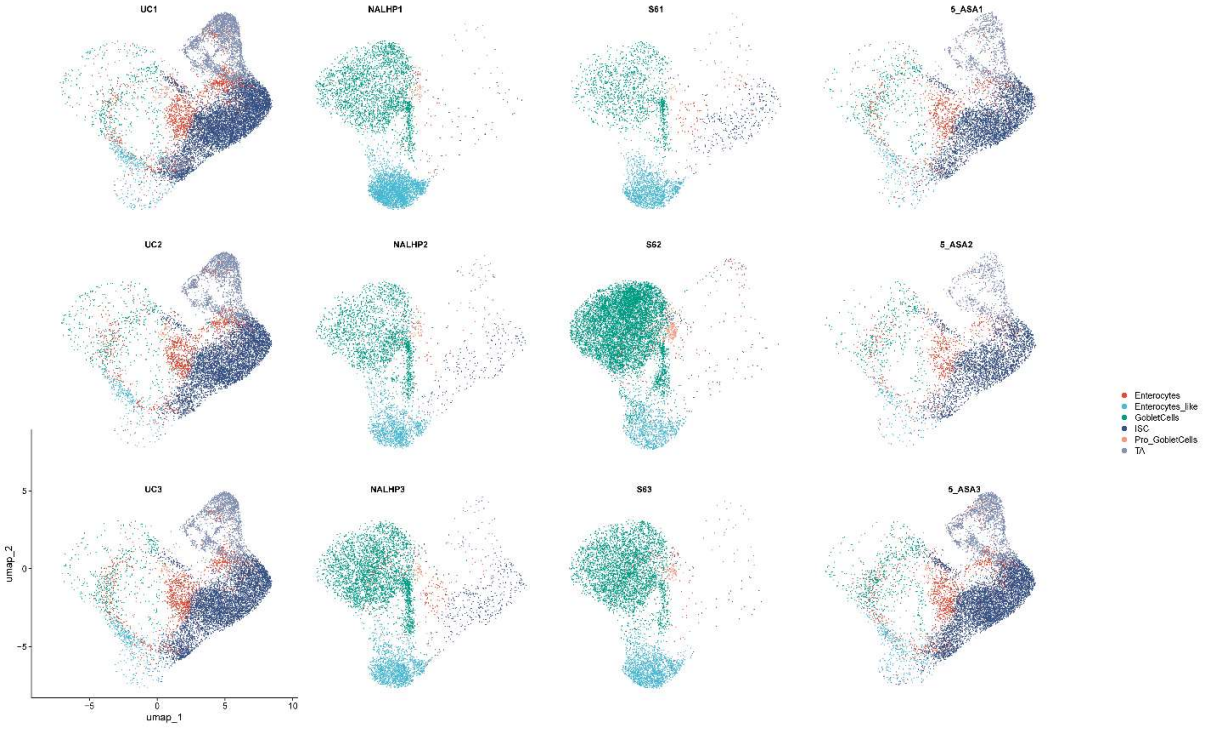

Dimensionality reduction of U-maps under the effects of NALHP, S6, and 5-ASA in three different UC patient derived UC organoids (UC1-UC3).

1209 **Extended Data Fig.18 | NCM460 cell fluorescence staining image**

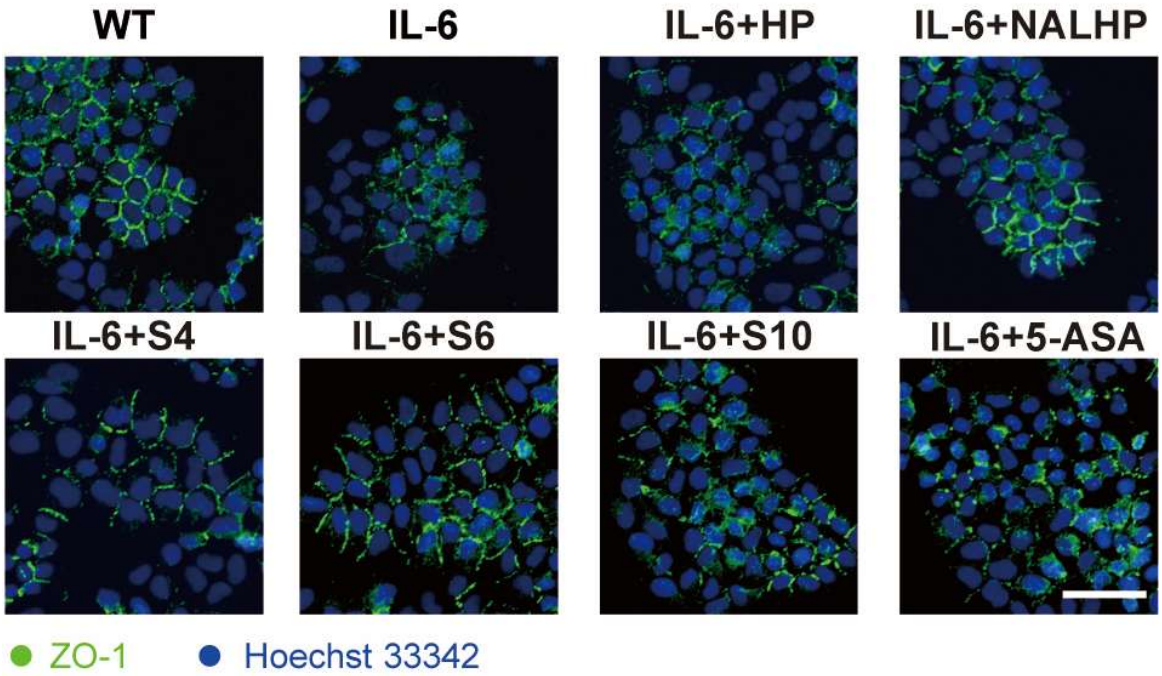

1210

1211 NCM460 cells were stimulated with IL-6 and treated with HP, NALHP, S4, S6, S10, 5-ASA (1

1212 mg/mL), scale bar=50 um. The expression level of ZO-1 protein was detected by fluorescent

1213 staining.

1214

1215 **Extended Data Fig.19 | Organoid transcriptomic analysis.**

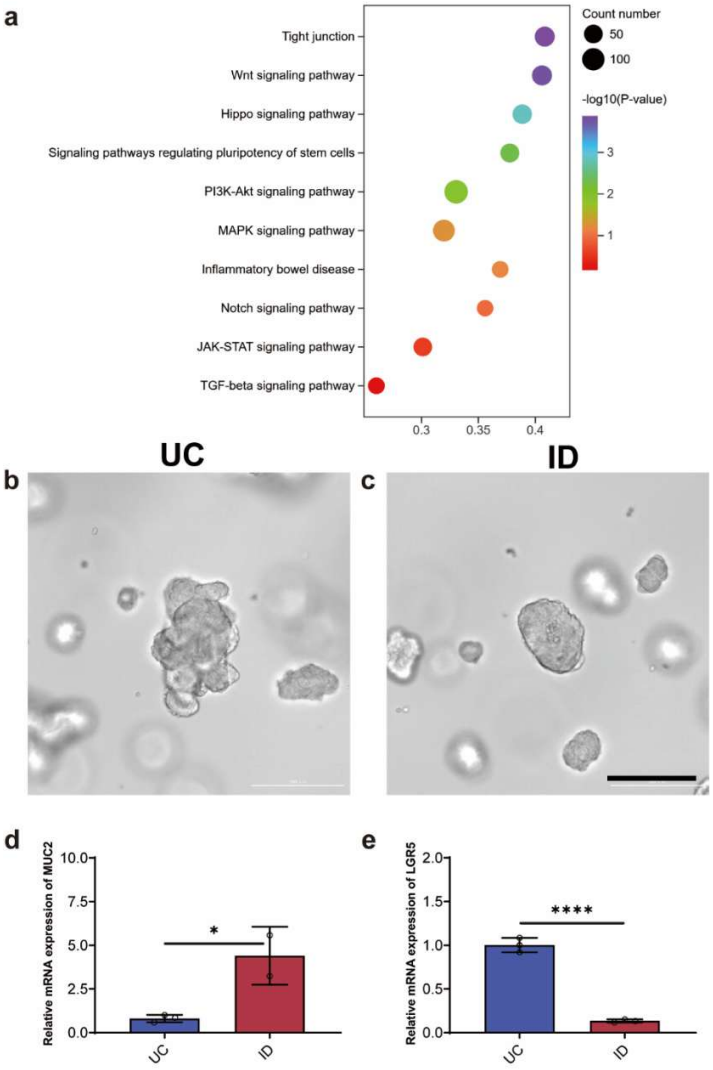

1216

1217 **a,** GO enrichment analysis of differentially expressed genes in UC organoids after NALHP

1218 treatment. **b,c,** Bright-field diagram of untreated (UC)(**b**) and under the treatment of IWP-2 and

1219 DAPT (ID)(**c**), scale bar=200 um. **d,e,** Relative mRNA expression of MUC2(**d**) and LGR5(**e**)

1220 under the treatment of IWP-2 and DAPT (ID).

1221

1222 **Extended Data Fig.20 | Bright-field diagram**

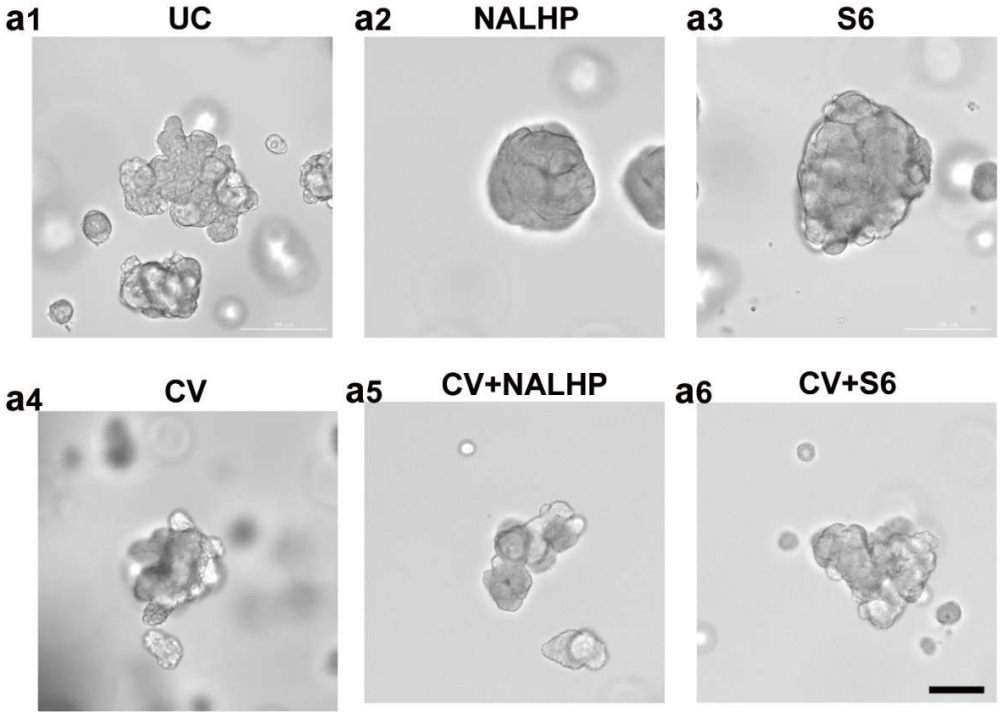

1223

1224

1225 UC organoids under the treatment of NALHP(a2), S6(a3), CV(a4), CV+NALHP(a5),

1226 CV+S6(a6), scale bar=200 um

1227

1228 **Extended Data Fig.21 | Expression of key proteins after NALHP/S6 and CHIR99021(C)**

1229 **and VPA(V) were co-cultured with UC organoids.**

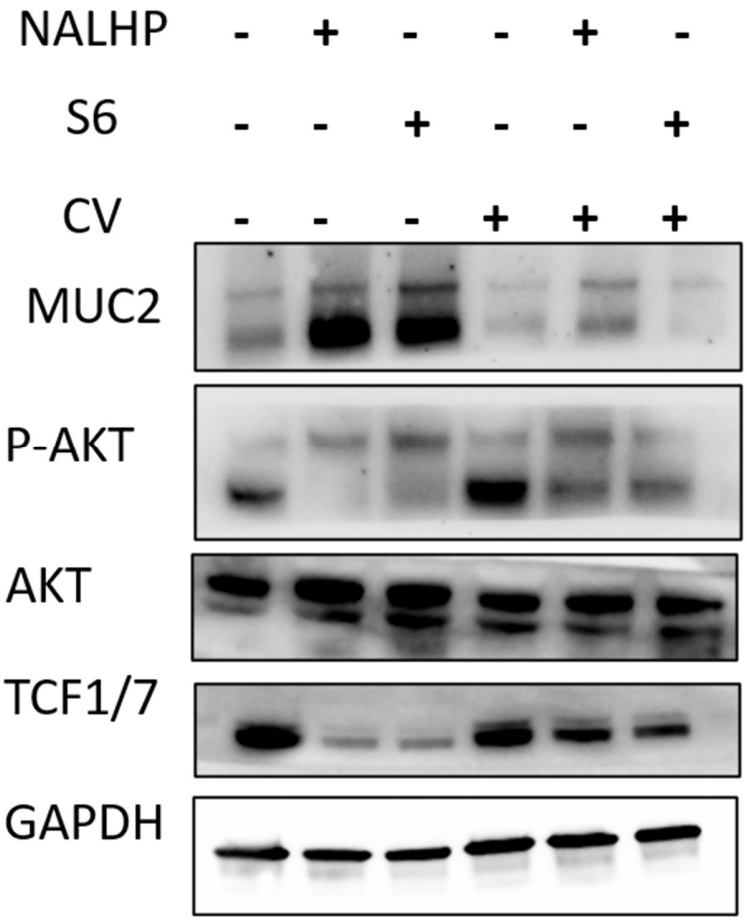

1230

1231

1232

1233

Extended Data Fig.22 | Expression of key proteins after NALHP/S6 and CHIR99021(C) were co-cultured with UC organoids.

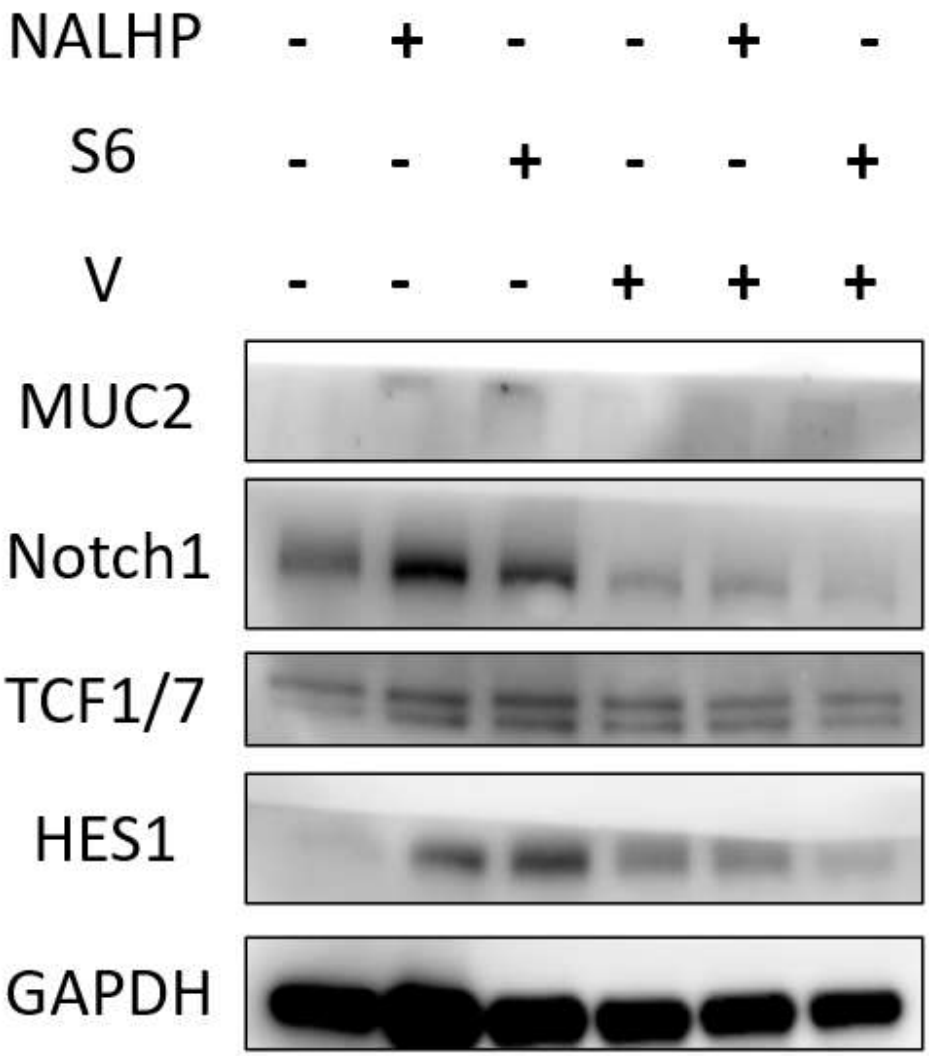

1238 **Extended Data Fig.23 | Expression of key proteins after NALHP/S6 and VPA(V) were co-**

1239 **cultured with UC organoids.**

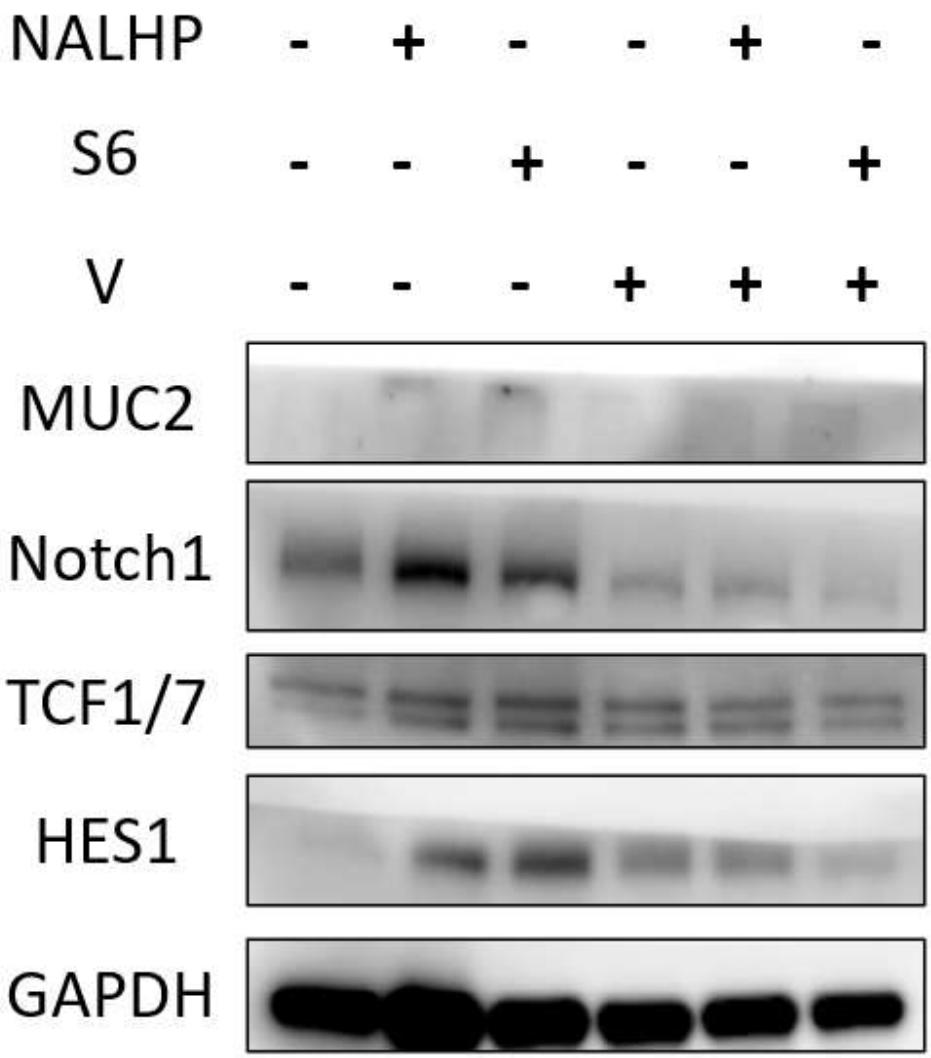

1240

1241

1242

Extended Data Fig.24 | Expression of key proteins after fondaparinux (Fonda) and non-anticoagulated fondaparinux (gs-Fonda) were co-cultured with UC organoids.

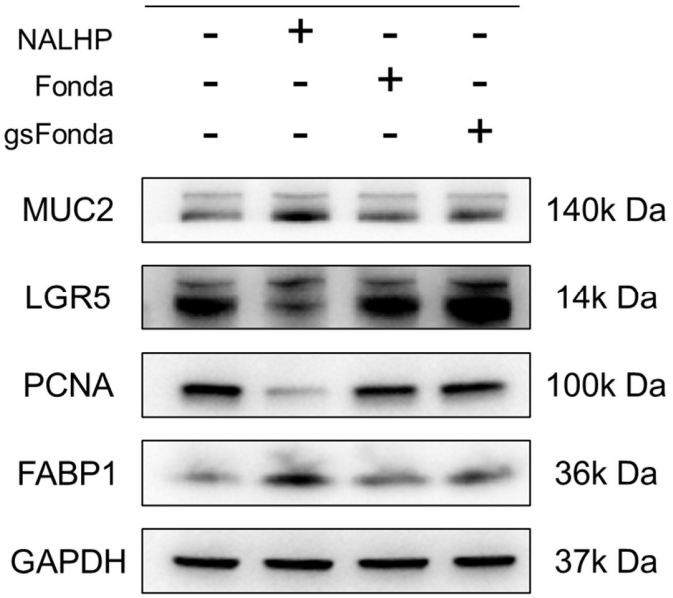

Extended Data is available for this paper.

Correspondence and requests for materials should be addressed to Xin-Hui Xing, Tel: 86-10-62794771, Email: xhxing@tsinghua.edu.cn, Yi Wang, Tel: 86-10-62773004, Email: wangyi671@mail.tsinghua.edu.cn, Xuan Jiang, Email: jiangxuan68@126.com